

On the origin of short-lived cocoon in 3C84: powered by tidal disruption events ?

NOZOMU KAWAKATU ^{1,2} MOTOKI KINO ^{3,4} AND WADA KEIICHI ^{2,5,6}

¹*Faculty of Natural Sciences, National Institute of Technology, Kure College, 2-2-11 Agaminami, Kure, Hiroshima, 737-8506, Japan*

²*Kagoshima University, Graduate School of Science and Engineering, Kagoshima 890-0065, Japan*

³*Kogakuin University of Technology & Engineering, Academic Support Center, 2665-1 Nakano, Hachioji, Tokyo 192-0015, Japan*

⁴*National Astronomical Observatory of Japan, 2-21-1 Osawa, Mitaka, Tokyo 181-8588, Japan*

⁵*Ehime University, Research Center for Space and Cosmic Evolution, Matsuyama 790-8577, Japan*

⁶*Hokkaido University, Faculty of Science, Sapporo 060-0810, Japan*

(Received May, 9, 2025; Revised June, 6, 2025; Accepted June, 28, 2025)

Submitted to ApJ

ABSTRACT

We evaluated the jet power and the density of ambient matter in 3C 84 by using the momentum balance along the jet axis and the transonic condition for the cocoons observed at two different scales (approximately 1 and 6 parsec scales). For the inner cocoon, we precisely determined the ratio of jet power to ambient density L_j/n_a to be $(0.3 - 0.7) \times 10^{43} \text{ erg s}^{-1} \text{ cm}^3$. Similarly, for the outer cocoon, we found that this value is more than an order of magnitude larger at $(0.9 - 3.7) \times 10^{44} \text{ erg s}^{-1} \text{ cm}^3$. This indicates that the outer cocoon is formed by a powerful jet that propagates through an ambient density of $20 - 300 \text{ cm}^{-3}$ with a jet power of $10^{45-46.5} \text{ erg s}^{-1}$. On the other hand, the inner cocoon is formed by a weaker jet with a power of $10^{43-44} \text{ erg s}^{-1}$, propagating through a relatively low-density environment of $6 - 20 \text{ cm}^{-3}$. These results suggest that: 1) with respect to the difference in n_a , it appears to support the hypothesis that the inner cocoon, recently formed about 10 years ago, is expanding in the low-density cocoon created by the jet emitted about 25-50 years ago. 2) to achieve the short-lived and high L_j that generated the outer cocoon, a large mass accretion rate must be required over a short period to activate the jet. These may imply the extreme accretion event driven by the tidal disruption events (TDEs) of massive stars and/or the disk instability.

Keywords: Active galactic nuclei (16)— Radio galaxies (1343)— Relativistic jets (1390)— Tidal disruption (1696)

1. INTRODUCTION

The formation of relativistic jets and their connection to the accretion disk remains a significant question in active galactic nuclei (AGN) physics (e.g., M. J. Rees 1984; M. C. Begelman et al. 1984). X-ray binaries, with their short dynamical timescales, provide a useful analogy for AGN jets. They show that the jet power may depend on the physical state of the accretion disk and the accretion rate (e.g., R. P. Fender et al. 2004; J. E. McClintock & R. A. Remillard 2006). The jet power in AGNs is correlated with narrow emission line luminosities, indicating a link between jet launching mechanisms and the accretion disk (e.g., S. A. Baum & T. Heckman 1989; S. Rawlings & R. Saunders 1991). However, interpreting this connection is challenging due to the long lifetimes of AGN jets, compared to rapid changes in accretion disk states (e.g., C. P. O’Dea et al. 2009). Furthermore, estimating the power of AGN jets L_j is difficult because most emissions from AGN jets are from non-thermal electrons, obscuring signals from thermal and proton components.

To solve this issue, jet power can be estimated by measuring cavity volumes and buoyant rise times for low-power Fanaroff-Riley I (FR I) radio galaxies (e.g., L. Birzan et al. 2004; D. A. Rafferty et al. 2006; B. R. McNamara et al. 2011; H. R. Russell et al. 2013). In contrast, high-power Fanaroff-Riley II (FR II) radio galaxies have cocoons with pressures exceeding the surrounding gas, allowing for jet power estimation through cocoon dynamics (e.g., M. C. Begelman & D. F. Cioffi 1989; C. R. Kaiser & P. Alexander 1997; M. Kino & N. Kawakatu 2005; H. Ito et al. 2008). However, it is difficult to examine early jet formation stages, which is closely related to the physical state of the accretion disk, because these estimates are the averaged jet power over typical ages of FRIs and FRIIs, i.e., 10^{6-8} yrs. Therefore, estimating L_j for much younger compact radio galaxies is essential.

Compact symmetric objects (CSOs), whose sizes are from 10 pc to 1 kpc, are crucial for studying the early stage of jet formation, because CSOs with ages of 10^2 to 10^5 years are much younger than typical radio galaxies such as FRIs and FRIIs (e.g., C. P. O’Dea 1998; M. J. Hardcastle & J. H. Croston 2020; C. P. O’Dea & D. J. Saikia 2021; A. C. S. Readhead et al. 2024). Observations show that CSOs represent a large fraction ($\sim 30\%$) in the flux-limited catalog of radio sources (C. Fanti et al. 1995), which is much higher than the expected value ($< 0.1\%$) of their ages. This suggests that a large fractions of CSOs stop their jet activity at an early stage of their evolution $< 10^5$ yr (C. S. Reynolds & M. C. Begelman 1997; P. Alexander 2000; M. Orienti & D. Dallacasa 2020; A. Marecki et al. 2003; N. E. Gugliucci et al. 2005; M. Kunert-Bajraszewska et al. 2010; M. Orienti et al. 2010; M. L. Lister et al. 2020; K. Nyland et al. 2020; M. Kunert-Bajraszewska et al. 2020; A. Wołowska et al. 2021). Recently, S. Kiehlmann et al. (2024a) have shown that the edge-brightened high luminosity CSOs form a distinct subclass of jetted AGN that has a sharp upper cutoff in size at $\simeq 500$ pc based on the complete sample (S. Kiehlmann et al. 2024b). Thus, many CSOs may be short-lived (e.g., A. C. S. Readhead et al. 1994, 2024). Therefore, clarifying not only the jet power L_j but also the time variability of the jet power $L_j(t)$ are essential to reveal the origins of CSOs.

To obtain the total kinetic power L_j for CSOs, the estimation of ambient density around CSOs, $n_a(r)$ plays a crucial role. However, it is challenging to estimate the ambient density within galaxies because the emission from diffuse ambient gas is very weak because of contamination from other bright sources. According to the dynamical model of the expanding cocoon and the shell, the expansion velocity strongly depends on the ambient density (e.g., C. S. Reynolds & M. C. Begelman 1997; C. S. Reynolds et al. 2002; S. S. Komissarov et al. 2007; B. B. Nath 2010; P. Mocz et al. 2011; M. Perucho et al. 2011; H. Ito et al. 2015). Thus, if the expansion velocity is obtained from observations, it is possible to constrain the ambient density.

The nearby bright radio galaxy 3C 84 ($z = 0.0176$), located at the center of the Perseus cluster and harboring a supermassive black hole (SMBH) with a mass of $M_{\text{BH}} = (0.8 - 2) \times 10^9 M_{\odot}$ (J. Scharwächter et al. 2013; G. Giovannini et al. 2018), provides an ideal environment for studying the physics of energy transport by radio lobes at parsec scales. Since a pair of jets has been observed on scales ranging from sub-pc to 10 kpc scale (e.g., R. Morganti et al. 2023), we recognize that 3C 84 is an extreme case which exhibits intermittent jet ejections. In the central region of 3C 84, single-dish observations of 3C 84 showed that the outburst started in 1959 and found two types of variations; one is fast outbursts happen at radio frequencies 5 years after the corresponding optical flares. The rapidly varying lasts from several months in the optical and a few years at radio band. The other is the slowly varying component which has a timescale of about 30 years. This slow variation leads to the growth and decay of the radio emitting jets (e.g., N. S. Nesterov et al. 1995). By using a six-station VLBI network, A. C. S. Readhead et al. (1983) revealed compact radio structure, which may be related to the radio outburst in 1959. Recently, much more compact radio sources were discovered within the outer 6 pc-scale radio cocoon (hereafter we call it the outer cocoon) observed by VLBI Space Observatory Program (VSOP) observations (K. Asada et al. 2006). The C3 component in 3C 84 is identified as a newborn radio lobes started in 2005 and it propagates southward (e.g., H. Nagai et al. 2010).

These radio morphologies in the central 10 pc scale region are quite similar to that of CSOs. Thus, it is useful to understand the origin of CSOs because the compact (< 10 pc) cocoons may be the early phase of more extended CSOs whose size is from 10 pc to kpc. Recently, using 5GHz *RadioAstron* space-VLBI observations, T. Savolainen et al. (2023) reported the first discovery of a cocoon-like, low-intensity, emission structure surrounding the parsec-scale restarted jet of the 3C 84 (hereafter we call it the inner cocoon). These findings indicate that we can investigate whether there are variations in jet power over a short period for the inner and outer cocoons in 3C 84, $L_j(t)$. However, this has been challenging due to significant uncertainties in the surrounding ambient gas density within < 10 pc in order to examine the jet power on a parsec scale. In this paper, we will assess the density of ambient gas using the expansion velocity of the cocoon and the shell, as seen in Figure 1.

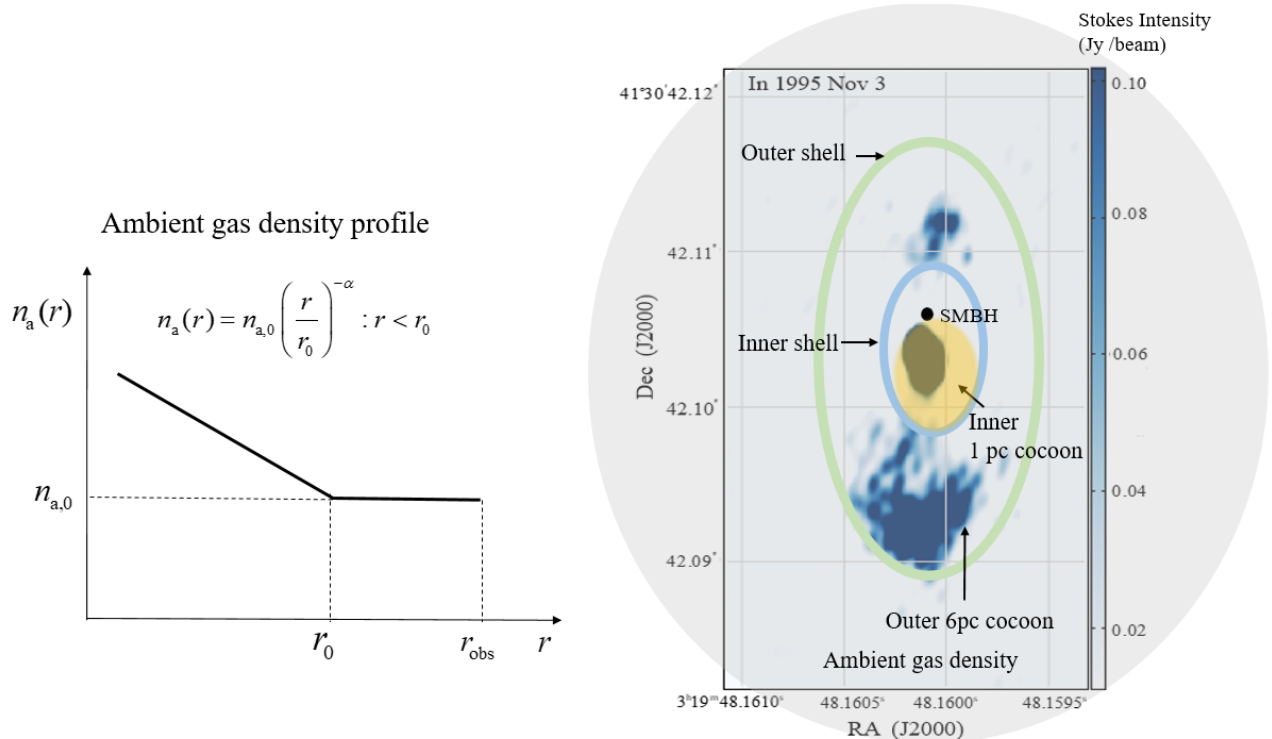


Figure 1. Left: A sketch of the expected surrounding gas density profile. The vertical axis is the number density of ambient gas $n_a(r)$. The horizontal axis is the distance from the SMBH, r . $n(r_{a,0}) = 0.1 \text{ cm}^{-3}$ is the density observed at $r = r_0 = 1 \text{ kpc}$, r_0 is the critical radius of the gas density and α is the slope index of $n_a(r)$ for $r < r_0$. Right: A cartoon of the multiple mini-cocoon/radio-lobe/shell system overlaid on the radio image of 3C 84. The large gray circle represents the ambient gas surrounding the entire system. The outer cocoon is depicted as white-colored bubbles. The current expanding velocity of outer cocoon/shell is subsonic (See Figure 2 for details). As for the inner lobe, it is well known that the northern inner lobe is significantly affected by free-free absorption of ionized plasma near the central SMBH, making the northern inner lobe not clearly visible (e.g., R. C. Walker et al. 2000; K. Wajima et al. 2020). Therefore, it is not depicted in this sketch. The small orange-colored bubble is the inner cocoon surrounding the parsec-scale newborn jet observed using 5GHz *RadioAstron* space-VLBI observations (T. Savolainen et al. 2023). The expanding velocity of inner cocoon/shell is still supersonic. The blue and green rings represent the inner and outer shells, respectively.

The goal of this paper is to estimate the kinetic jet power and ambient density around parsec-scale multiple jets in 3C 84, based on the conditions of supersonic and subsonic expansion of cocoons. In Section §2, the method, problem setting, and dynamical model in the AGN cocoon and shell are briefly described. In Section §3, we present the results. We provide a discussion in §4. The summary is given in Section §5. With the cosmology parameters of $\Omega_m = 0.27$, $\Omega_\Lambda = 0.73$, and $H_0 = 71 \text{ km s}^{-1} \text{ Mpc}^{-1}$ (E. Komatsu et al. 2009) the angular scale of 1 mas corresponds to a linear distance of 0.35 pc for 3C 84.

2. MODEL OF COCOON/SHELL EXPANSION IN 3C 84

2.1. Problem setting and basic idea of the method

Details of the dynamical model of over-pressured cocoon's expansion (e.g., M. C. Begelman & D. F. Cioffi 1989; M. Kino & N. Kawakatu 2005) and shell (H. Ito et al. 2015) have been established. In this paper, we apply these well-established models for simplicity. In models, the physical quantities of the cocoon and shell are expressed as functions of L_j and the age of the cocoon t_{age} . However, here we can treat the physical quantities of cocoon and shell as given by L_j because t_{age} of mini-cocoon is well constrained by observations.

In Figure 1, we present a cartoon of the multiple mini-cocoon/shell system observed in 3C 84. The kinetic energy of the jets is dissipated through the termination shock at the hot spots and deposited into the cocoon and the shell with its width. The cocoon is inflated by its internal energy. The cocoon drives the forward shock propagating in the ambient gas, and the forward-shock region forms the shell. The model parameters are the jet power, L_j and the

Table 1. Physical quantities in 3C84

Quantities	Symbol	Note
Jet kinetic power	L_j	model parameter
Distance from the SMBH to the cocoon head	R_h	1.4 - 4 pc for inner cocoon 5.6 - 15.7 pc for outer cocoon
Velocity of cocoon head	$v_h(r)$	observable parameter
Velocity of cocoon head at $r = r_0$	$v_{h,0}$	observable parameter
Cross-sectional area of cocoon/lobes	$A_h(r)$	observable parameter
Cross-sectional area of cocoon/lobes at $r = r_0$	$A_{h,0}$	observable parameter
Shell/cocoon radius	$R(t)$	model parameter
Expanding shell velocity	$\dot{R}(t)$	model parameter
Growth rate of the cocoon head	β	1 (parabolic case) , 2 (conical case)
Age of cocoons	t_{age}	observable parameter
Duration of jet injection	t_j	free parameter
Transonic timescale	t_{trans}	Eq. (7)
Number density of ambient gas	$n_a(r)$	model parameter
Number density of ambient gas at $r = r_0$	$n_{a,0}$	0.1 cm^{-3} at $r = r_0$
Critical radius of ambient gas density	r_0	10 pc, 100 pc and 1 kpc
Power-law index of ambient gas density	α	0.5-2

number density of the spherically symmetric ambient gas, $n_a(r)$ where r is the distance from the SMBH. Here, L_j takes into account the possibility of a change between the formation of the two cocoons, but L_j is assumed to be constant during each cocoon formation. Table 1 summarizes the physical quantities used in our model. Among them, the obtained quantities are the velocity of the cocoon head $v_h(R_h)$, the cross-sectional area of the cocoon $A_h(R_h)$, and the age of the cocoon t_{age} , where R_h is the distance from the SMBH to the cocoon head. The free parameters are the critical radius r_0 and the power law index α , which determine the profile of the ambient gas density (see Table 1). Thus, we can constrain L_j and $n_a(R_h)$, since the basic equations are two: the momentum balance along the jet axis and the subsonic condition of the expanding shell.

The method is divided into four steps as follows: (i) In Section 2.2, we analyzed three epochs of VLBA archival data of 3C 84 at 15 GHz obtained in 1995, 2015 and 2022 to understand the basic characteristics of both inner and outer cocoons. (ii) We specify the properties of the surrounding gas in Section 2.3, assuming that the ambient gas density is closely related to the evolution of the shell/cocoons. (iii) The ratio of the total jet power to the ambient density, $L_j/n_a(R_h)$ is determined by the momentum balance along the jet axis in Section 2.4. Using the observed properties of cocoons, namely, the advance speed of the cocoon head, v_h and the cross-sectional area of the cocoon, A_h and the age of the cocoon t_{age} , we constrain $L_j/n_a(R_h)$ for each cocoon. (iv) We constrain the ambient gas density under the condition that the velocity of the expanding shell/cocoon is the sound velocity of the surrounding gas in Section 2.5. Recent observations suggest that the inner cocoon expands supersonically, while a pair of fading outer radio lobes expands subsonically, as shown in Figure 2. Finally, the jet power L_j for the inner and outer cocoons is used to estimate how $L_j(t)$ changes in time.

2.2. Inner and outer cocoons of 3C 84 images at 15 GHz

To understand the basic characteristics of the cocoons, we displayed three epochs of relatively good quality VLBA archival data of 3C 84 at 15 GHz obtained in 1995, 2015, and 2022 (project IDs are BR12, BL193AS, and BL286AK, respectively). These three were adopted from already analyzed MOJAVE images (<http://www.physics.purdue.edu/MOJAVE/>). In Figure 2, we show the obtained intensity map of the inner and outer radio cocoon/lobes. The image root mean square (rms) (1σ) values are 11.12 mJy/beam (BA12), 1.04 mJy/beam (BL193AS), 4.44 mJy/beam (BL286AK), respectively. The typical spatial resolution is the dimensions of 1.1 mas \times 0.5 mas (M. L. Lister et al. 2018). We find that the total flux of the northern and southern lobes has decreased tenfold

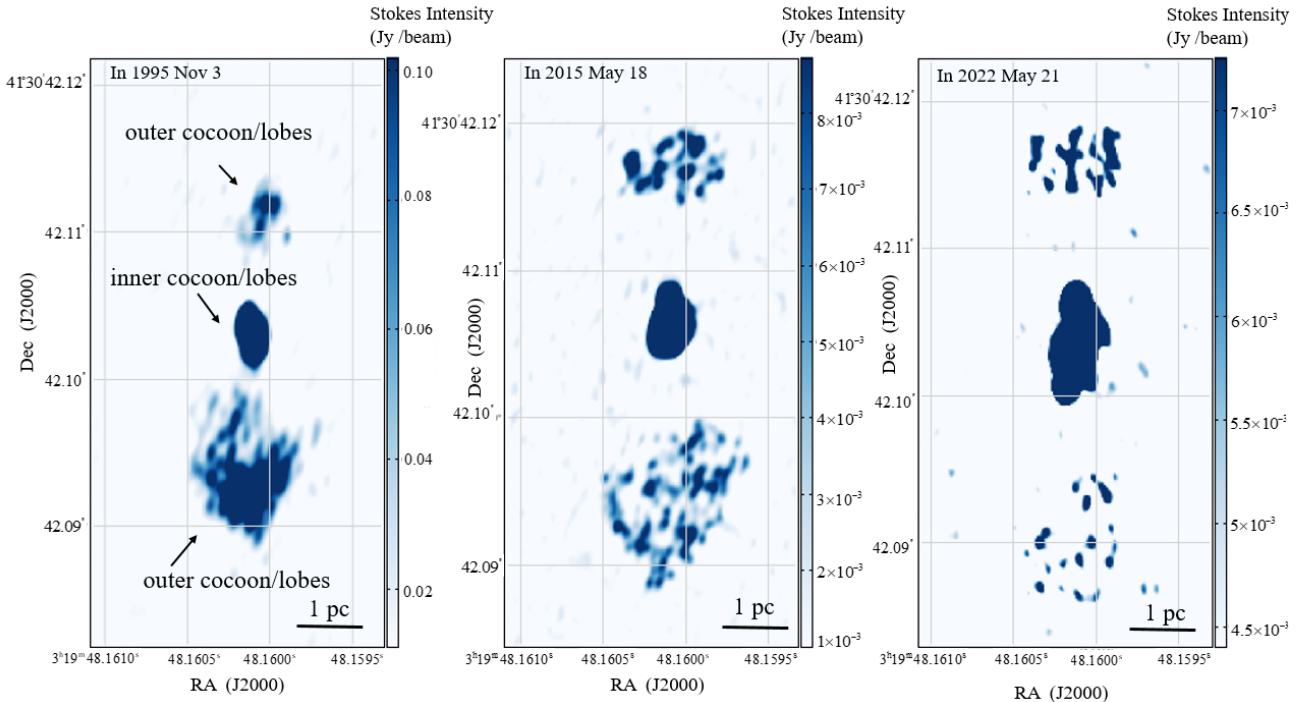


Figure 2. Comparison of the three epochs of the actual 3C 84 images at 15 GHz taken from the MOJAVE project (<https://www.cv.nrao.edu/MOJAVE/>) in 1995 Nov 3, 2015 May 18, and 2022 May 21, with the project IDs, BA12, BL193AS, BL286AK, respectively. The image rms (1σ) are 11.12 mJy/beam (BA12), 1.04 mJy/beam (BL193AS), 4.44 mJy/beam (BL286AK), respectively. Typical spatial resolution is the dimensions of 1.1 mas \times 0.5 mas (M. L. Lister et al. 2018), where the angular scale of 1 mas corresponds to a linear distance of 0.35 pc. Corresponding to Figure 1, the expanding central compact radio lobe with the size of 1 pc order (inner lobes/cocoon) and a pair of fading outer radio lobes with the size of 6 pc order (outer lobes/cocoon) are seen in these images.

over 20 years. In addition, we observe that the outer radiolobe morphology started to collapse after the epoch in 2015, and the expansion speed of the cocoon head should be subsonic because there is no evidence of lobe expansion from 2015 to 2021 (M. Kino et al. 2017). On the other hand, recent observations indicate that the expanding velocity of the inner cocoon is super-sonic (e.g., H. Nagai et al. 2010). As shown in Figure 1, the expanding central compact radio lobe with a size of approximately 1 pc (inner cocoon) and a pair of fading outer radio lobes with a size of about 6 pc (outer cocoon) are seen in these images.

2.3. Density profile of ambient gas

To study the evolution of mini-cocoon/shell, we need to specify the properties of the surrounding gas. Using the deep Chandra observation (A. C. Fabian et al. 2006), G. B. Taylor et al. (2006) estimated that the number density at $r_{\text{obs}} = 1$ kpc is $\simeq 0.1 \text{ cm}^{-3}$. However, there is no information on the gas for $r < 1$ kpc because the hot gas is strongly affected by the X-ray cavities created by past AGN activities and strong AGN feedback in the vicinity of the SMBHs. As seen in Figure 1, we postulate the density profile of ambient gas, $n_a(r)$ as follows;

$$n_a(r) = \begin{cases} n_{a,0} \left(\frac{r}{r_0}\right)^{-\alpha} & ; r < r_0 \\ n_{a,0} & ; r_0 \leq r < r_{\text{obs}}, \end{cases} \quad (1)$$

where α is the slope index of $n_a(r)$. Here, $n_{a,0} = 0.1 \text{ cm}^{-3}$ is the ambient gas density at $r = r_0$, and r_0 is the critical radius of the ambient gas density. Concerning the critical radius r_0 , we adopt three cases; the case (i) is $r_0 = 10$ pc, case (ii) is $r_0 = 100$ pc, and case (iii) is $r_0 = 10^3$ pc. In this paper, we focus on the diffuse hot gas that mainly interacts with the expanding mini-cocoon. The region along the jet axis is considered to be essentially free of gas clouds because there is no centrifugal force acting on gas clouds (e.g., C. Ramos Almeida & C. Ricci 2017). Thus, the clumpy gas clouds do not affect on the global jet propagation significantly, although a local collision between the jet and a compact

dense clouds at the central one-parsec region has been reported (M. Kino et al. 2021; M. Kam et al. 2024). We also assume the hot gas temperature around the galactic center ($r < 1$ kpc) is constant with $T_a = 3$ keV which is the gas temperature at $r \sim 1$ kpc (A. C. Fabian et al. 2006). The dependence of T_a will be discussed in Section 3.1.2.

For cases (i) and (ii), we propose a flat density profile for $r_0 < r < r_{\text{obs}}$, which may reflect a scenario in which the thermal instability of the gas is effective and most of the hot gas becomes cold gas (e.g., P. Barai et al. 2012; M. Gaspari et al. 2012; M. McCourt et al. 2012; P. Sharma et al. 2012; F. Guo & W. G. Mathews 2014; G. R. Meece et al. 2015). For the slope index α , we examine a wide range of parameter space, i.e., $\alpha = 0.5 - 2$. For the classical Bondi accretion, α is expected to be 1.5 from the mass conservation. On the other hand, in the context of advection-dominated inflow-outflow solution (i.e., the radiatively inefficient accretion flows (RIAF)-type hot accretion flows with substantial winds or mass loss), $0.5 \leq \alpha \leq 1.5$ was suggested by R. D. Blandford & M. C. Begelman (1999). Moreover, numerical simulations of a gravitational collapse in the presence of the gas cooling have shown that the slope is $0 < \alpha < 2$ (e.g., J.-H. Choi et al. 2013, 2015). For reference, we define characteristic radius such as the Bondi radius, r_B and the radius of the sphere of gravitational influence (SGI), r_{SGI} . Suppose that the central stellar velocity dispersion is $\sigma = 250$ km/s (D. Bettoni et al. 2003) and the mass of the central black hole is $M_\odot = 8 \times 10^8 M_\odot$ (J. Scharwächter et al. 2013), r_B and r_{SGI} are $r_B = 2GM_{\text{BH}}/c_s^2 = 12$ pc and $r_{\text{SGI}} = 2GM_{\text{BH}}/\sigma^2 = 60$ pc where c_s is the sound velocity of the ambient gas with T_a .

2.4. Evolution of the cocoon

The over-pressured cocoon model was initially proposed by M. C. Begelman & D. F. Cioffi (1989), where the dissipated energy of the jet bulk motion is the origin of the total pressure of the cocoon (e.g., C. R. Kaiser & P. Alexander 1997; M. Kino & N. Kawakatu 2005; Y. Fujita et al. 2016b). A supersonic cocoon is expected to be over-pressured against ambient pressure with a significant sideways expansion. Thus, in general, we need to solve three basic equations: the equation of motion along the jet axis, sideways expansion, and energy conservation in the cocoon. However, thanks to the well-constrained quantities of the mini-cocoon by observations (see Table 1), it is sufficient to consider only the evolution of the cross-sectional area of the cocoon A_h and that of the expanding speed of the cocoon v_h . Since v_h is about 10% of light speed c (e.g., N. Kawakatu et al. 2008), the relativistic effect on the cocoon evolution is negligible. The momentum balance along the jet is given by :

$$\frac{L_j}{v_j} = m_p n_a(r) v_h(r)^2 A_h(r), \quad (2)$$

where L_j , v_j , m_p , v_h and A_h are the kinetic power of jets, the velocity of jet, the proton mass, the advance velocity of cocoon, and the cross-sectional area of cocoon head, respectively. We assume that the velocity of jets are relativistic speed, i.e., $v_j = c$ because the bulk Lorentz factor $\Gamma = (1 - (v/c)^2)^{-0.5}$ is larger than 3 (e.g., G. Giovannini et al. 2018). The growth rate of A_h is assumed to be merely a power law as

$$A_h(r) = A_{h,0} \left(\frac{r}{r_0} \right)^\beta, \quad (3)$$

where β is the power law index of $A_h(r)$. We here assume two cases: $\beta = 1$ is the parabolic case and $\beta = 2$ is the conical case. Thus, the ratio of jet power to ambient density is given by $L_j/n_a(r) = m_p v_h(r)^2 A_h(r) c$. Note that the physical quantities A_h and v_h are observable in the right hand of above equation (Eq.(2)). In addition, the velocity of the cocoon head is expressed as

$$v_h(r) = v_{h,0} \left(\frac{r}{r_0} \right)^{\frac{\alpha - \beta}{2}}. \quad (4)$$

From Eqs. (2), (3) and (4), we obtain the time t as a function of r as

$$t(r) = \frac{2r}{2 - \alpha + \beta} \left(\frac{L_j}{m_p n_a(r) A_h(r) c} \right)^{-1/2}, \quad (5)$$

which is consistent with the results (Y. Fujita et al. 2016b; Y. Fujita & H. Nagai 2017) for $\beta = 2$. We should note that the age of the cocoon t_{age} is the time at $r = R_h$.

2.5. Evolution of shell

To treat the dying phase of the outer cocoon as seen in Figure 2, we consider the evolution of the expanding shell. After stopping jet energy injection, that is, $L_j = 0$ for $t > t_j$, the cocoon will rapidly lose its energy due to adiabatic expansion and transfer most of its energy to the shell within a dynamical timescale, where t_j denotes the duration of jet injection (H. Ito et al. 2015). For the phase after the jet has been turned off ($t > t_j$), the expansion of the bow shock (shell) is expected to be similar to the Sedov-Taylor solutions. The radius of the shell $R(t)$ is given by

$$R(t) = R(t_j) \left(\frac{t}{t_j} \right)^{\frac{2}{5-\alpha}}. \quad (6)$$

Here $R(t_j) = C(L_j/(m_p n_{a,obs}))^{1/(5-\alpha)} r_0^{\alpha/(\alpha-5)}$, where C is the numerical coefficient and the explicit form of $C = [(3-\alpha)(5-\alpha)^3(\gamma_c-1)/4\pi(2\alpha^2+\alpha-18\gamma_c\alpha+63\gamma_c-28)]^{1/(5-\alpha)}$ where $\gamma_c = 4/3$ since plasma within the cocoon is expected to be relativistic. On the other hand, the transonic condition of the expanding shell velocity $\dot{R}(t = t_{trans})$ is

$$\dot{R}(t = t_{trans}) = c_s, \quad (7)$$

where

$$t_{trans} = \left(\frac{C}{c_s} \right)^{\frac{5-\alpha}{3-\alpha}} \left(\frac{L_j}{m_p n_{a,0} r_0^\alpha} \right)^{\frac{1}{3-\alpha}} t_j^{\frac{1}{3-\alpha}}. \quad (8)$$

The sound velocity of the ambient gas is given by $c_s = (k_B T_a / \mu m_p)^{1/2}$ where k_B and $\mu = 0.6$ are the Boltzmann constant and the mean molecular weight of the ambient gas. Here we assume that c_s is constant. Combining Eqs.(7) and (8), the above transonic condition can be rewritten as

$$\left(\frac{L_j}{n_{a,0}} \right)_{trans} = C^{\alpha-5} c_s^2 m_p R_h^3 t_j^{-1} \left(\frac{r_0}{R_h} \right)^\alpha, \text{ where } R(t = t_{trans}) = R_h. \quad (9)$$

The velocity of the shell is expressed as $(E_j/M_s)^{1/2}$ where the total energy $E_j = L_j t_j$ and the swept mass of the shell M_s . Thus, the dependence of $(L_j/n_{a,0})_{trans}$ on t_j and R_h is easily understood. As r_0 and α become larger, $n_a(R_h)$ increases. Since larger $n_a(R_h)$ cause a strong deceleration of the shock velocity, higher $(L_j/n_{a,0})_{trans}$ is required for given R_h .

3. RESULTS

We first constrain the ratio of jet power to ambient gas density $L_j/n_a(R_h)$ using the momentum balance along the jet axis. Applying the transonic condition, we constrain the slope index α and the critical radius r_0 of the ambient gas density. Next, we evaluate the ambient gas density profile $n_a(r)$ for both inner and outer cocoons. Finally, we estimate the jet power, L_j , associated with the inner and outer cocoons and discuss how the jet power in 3C 84 changes in the last 50 years.

3.1. Constraint on $L_j/n_a(R_h)$ and $n_a(R_h)$

3.1.1. Allowed L_j/n_a

Figure 3 shows the ratio of $L_j/n_a(R_h)$ as a function of the ambient gas density profile, α and the age, t_{age} for a given jet head growth rate ($\beta = 1$: parabolic shape). The black lines represent different ages of the inner cocoon with $t_{age} = 8, 10, 12, 15, 20,$ and 25 yr, respectively (see Eq. (5)). Only by the momentum balance along the jet (Eq.(2)), the allowed region is obtained as $L_j/n_a(R_h) = (0.3 - 1.6) \times 10^{43} \text{ergss}^{-1} \text{cm}^{-3}$ using the observed values with $v_h = 0.23 - 0.55 c$ and $A_h = 0.13 - 0.39 \text{pc}^2$ at $R_h = 1.4 - 4 \text{pc}$ (T. Savolainen et al. 2023) for the wide range of the jet inclination angle $\theta = 18^\circ - 65^\circ$ (M. L. Lister et al. 2009; H. Nagai et al. 2010; K. Suzuki et al. 2012; Y. Fujita & H. Nagai 2017) Next, we further constrain the ratio of $L_j/n_a(R_h)$ and the slope index α by incorporating the allowed range of the observed cocoon age t_{age} and the advance velocity of the cocoon $v_h(t)$. We estimate the age of the inner cocoon t_{age} in September 2013, when the 5 GHz image was taken by *Radioastron*. According to K. Suzuki et al. (2012), the new-born hot spot "C3" was first identified in November 2003 and the initial velocity is $0.09 \pm 0.04 \text{mas/yr}$. In addition, the physical distance from the SMBH is 0.15 mas, considering the effect of the core shift (G. F. Paraschos et al. 2021). Combining these values, the age of the inner cocoon can be very constrained to $t_{age} = 12 - 15 \text{yr}$.

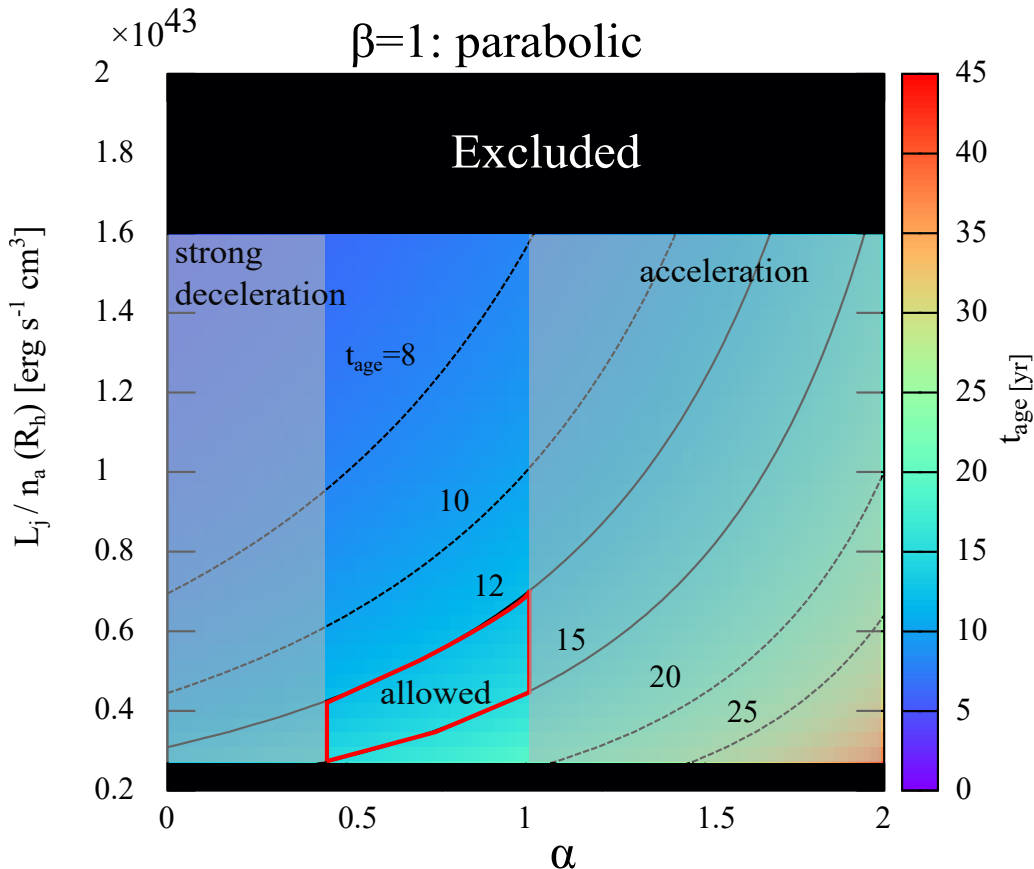


Figure 3. Contour plots of inner cocoon ages, t_{age} as functions of the ratio of jets and ambient density at R_h , $L_j/n_a(R_h)$ and the slope index of ambient density, α for the growth rate of the cocoon head with $\beta = 1$ (parabolic shape). The black lines represent different ages with $t_{\text{age}} = 8, 10, 12, 15, 20$ and 25 yr, respectively. The red outline represents the allowed range of $L_j/n_a(R_h)$ and α of the inner cocoon in 3C 84. The black filled area denotes the excluded range of $L_j/n_a(R_h)$ by the momentum balance along the jet axis. The light gray areas are excluded from the range of α because v_h is almost constant.

For $v_h(t)$, solutions exhibiting large deviations from constant velocity are safely ruled out from the VLBI observations (H. Nagai et al. 2010; K. Suzuki et al. 2012). Thus, we impose the condition that the expansion speeds v_h at 0.1 pc must be smaller than c for $v_h(R_h) = 0.5c$. As a result, we find that a smaller slope index, $\alpha = 0 - 0.4$, corresponds to a rapid deceleration in v_h , while a larger $\alpha = 1 - 2$ denotes an acceleration in v_h (see Eq. (4)). Thus, we can constrain the allowed range of the slope index α to $\alpha = 0.4 - 1$.

Combining the momentum balance along the jet axis, the observed range of t_{age} and the allowed range of α , we tightly constrain $L_j/n_a(R_h)$. The allowed range of $L_j/n_a(R_h)$ is obtained as

$$\left(\frac{L_j}{n_a(R_h)}\right)_{\text{inner}} = (0.3 - 0.7) \times 10^{43} \text{ ergs s}^{-1} \text{ cm}^{-3}, \quad (10)$$

which is highlighted as the red area in Figure 3. Figure 4 shows the allowed range of $L_j/n_a(R_h)$ with the growth rates of the jet head ($\beta = 2$: conical shape). Similarly, the allowed range of α is $\alpha = 1.4 - 2$. Compared to Figure 4, we confirm that the allowed range of $L_j/n_a(R_h)$ shows little dependence on the growth rate of A_h , i.e., β .

K. Asada et al. (2006) conducted VLBI Space Observatory Program (VSOP) observations of 3C 84, revealing details of the structure of radio lobes. Given that we can obtain key physical quantities such as $A_h(R_h) = 2 - 5.9 \text{ pc}^2$ and

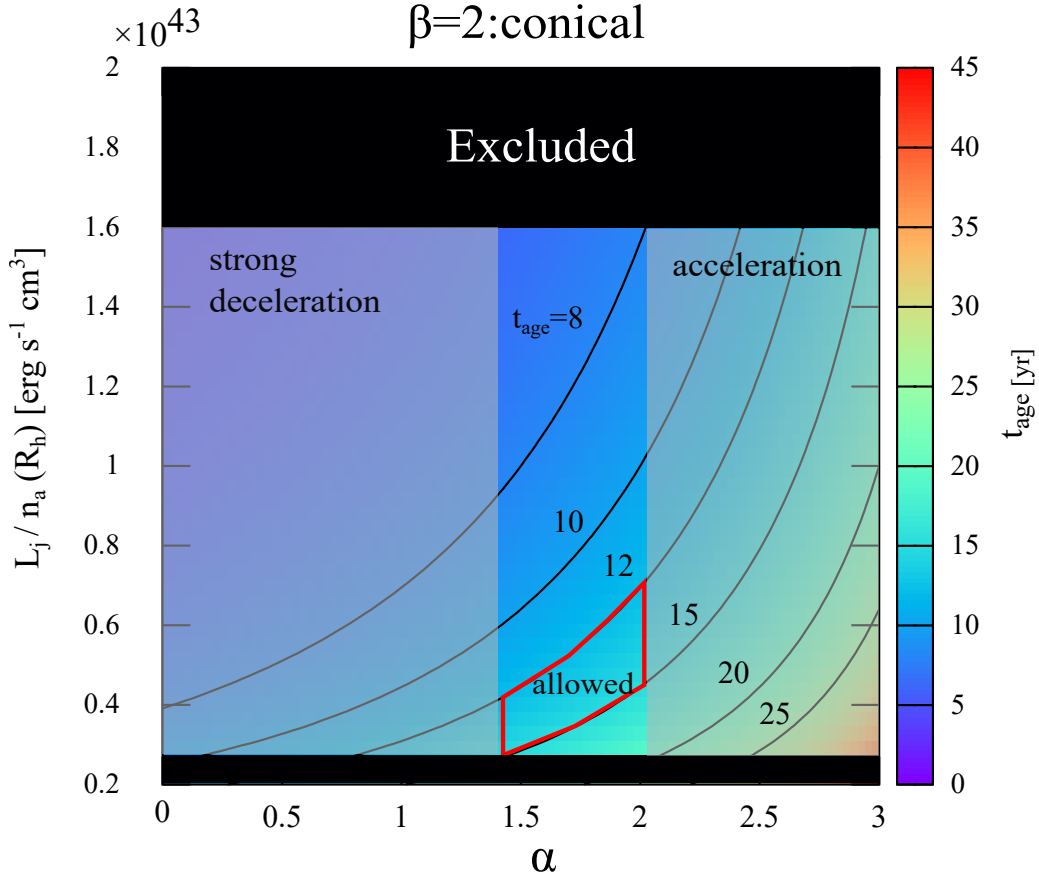


Figure 4. Same as Figure 3, but for the growth rate of the inner cocoon head with $\beta = 2$ (conical shape).

$v_h(R_h) = 0.2 - 0.4c$ where $R_h = 5.6 - 15.7$ pc, the ratio of L_j/n_a can be determined by the momentum balance along the jet axis (see Eq.(2)) as

$$\left(\frac{L_j}{n_a(R_h)}\right)_{\text{outer}} = (0.9 - 3.7) \times 10^{44} \text{ ergs s}^{-1} \text{ cm}^{-3}, \quad (11)$$

which is an order of magnitude larger than that of the inner cocoon and is consistent with previous studies (Y. Fujita et al. 2016b).

3.1.2. Allowed α

Figure 5 shows the ratio of jet power and ambient density, $L_j/n_a(R_h)$, as a function of the slope index of ambient density, α for the outer cocoon. The black lines show the transonic condition (Eq. (9)) for different critical radii $r_0 = 10$ pc, 100 pc and 10^3 pc with $t_j = t_{\text{age}} = 50$ yr and $R_h = 6$ pc. It is hard to accurately estimate the duration of the jet injection (t_j) or, equivalently, the time when the jet stopped because it is not a direct observable. However, we shortly discuss the lower value of t_j . The outer fading cocoon clearly indicates that t_j is shorter than t_{age} of the outer cocoon, where the range of t_{age} is $\simeq 45 - 60$ yr (M. Kino et al. 2017). For the lower value of t_j , since the radio flux of the outer cocoon started to decline 25 -30 years later (N. S. Nesterov et al. 1995), $t_j = 25 - 30$ yr could be expected. On the other hand, a theoretical point of view, if $t_j \leq 0.5t_{\text{age}}$, the radio flux of the cocoon decrease by an order of magnitude because of the Synchrotron cooling (H. Ito et al. 2015). Thus, the lower value of $t_j = 25$ yr would

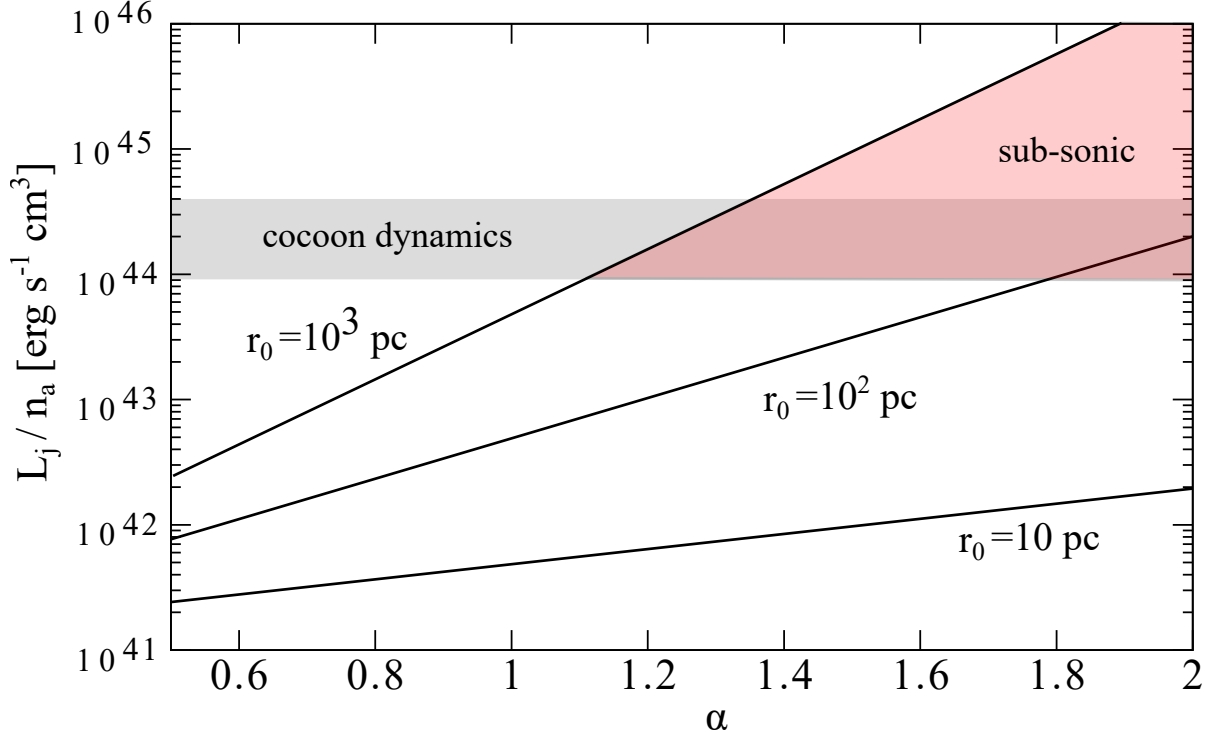


Figure 5. Condition of the subsonic expansion of the outer cocoon with $t_j = 50$ yr and $R_h = 6$ pc. The black lines represent the ratio of jet power and ambient density for the transonic condition (Eq. (9)) against α for the different critical radius, $r_0 = 10$ pc, 100 pc and 10^3 pc, respectively. The red area shows the allowed area, which is satisfied with the condition of the subsonic expansion. The grey area denotes the allowed $L_j/n_a(R_h)$ estimated by the momentum balance along the jet axis.

be reasonable. Even if a shorter duration, such as $t_j = 25$ yr, is adopted, our results do not change significantly because of $(L_j/n_a)_{\text{trans}} \propto t_j^{-1}$ (see Eq. (9)). If the observed value L_j/n_a is located above the line of $t_{\text{age}} = 50$ yr for given r_0 and α , it indicates that the expansion is subsonic (see Figure 2). The gray shaded area represents the allowed range of L_j/n_a derived from the cocoon dynamics, and the red-hatched region marks the areas satisfying the subsonic expansion conditions. As a result, we find that the slope index $\alpha = 1.1 - 2$ and $\alpha = 1.8 - 2$ are satisfied with the sub-sonic conditions for $r_0 = 10^3$ pc, $r_0 = 10^2$ pc, respectively. On the other hand, the subsonic expansion is not achievable for the case of $r_0 = 10$ pc because the ambient gas density is too low.

Figure 6 shows the supersonic conditions for the inner cocoon. The black lines show the transonic condition (Eq. (9)) for different critical radii $r_0 = 10$ pc, 100 pc and 10^3 pc with $t_j = t_{\text{age}} = 12$ yr and $R_h = 1.4$ pc. We should note that $t_j = 12$ yr is the lower limit because the inner cocoon still expands supersonically at present. This indicates that the slope index of the ambient density (α) must be relatively flat to maintain the supersonic expansion, that is, $\alpha = 0.5 - 0.8$ for $r_0 = 10^3$ pc and $\alpha = 0.5 - 1.2$ for $r_0 = 10^2$ pc. For $r_0 = 10$ pc, the supersonic condition matches all ranges of α , that is, $0.5 < \alpha < 2$. Therefore, to explain the dynamics of both the inner and outer cocoon/shell, the critical radius r_0 should be the range of $10 \text{ pc} < r_0 \leq 10^3 \text{ pc}$.

Lastly, we discuss the dependence of T_a and R_h . As seen in Eq. (9), the subsonic condition decreases with T_a due to $(L_j/n_a)_{\text{trans}} \propto T_a$. Thus, if $T_a = 10^4$ K, the subsonic solution for the outer cocoon disappears, which contradicts the radio observations, as seen in Figure 2. In addition, we assess how our results depend on R_h . Adopting the upper value of R_h , we find that the transonic condition is (2-6) times larger than the fiducial cases (Figures 5 and 6) because of $(L_j/n_a)_{\text{trans}} \propto R_h^{3-\alpha}$ (see Eq. (9)). Thus, this effect does not alter our main conclusion significantly, although the allowed range of α is slightly changed.

3.1.3. Allowed $n_a(R_h)$

As discussed in Section 3.1.2, we constrain the slope index of ambient gas with α for the outer cocoon (6 pc scale) and the inner cocoon (1 pc scale) by using the transonic condition of cocoon expansion. Thus, we here constrain the

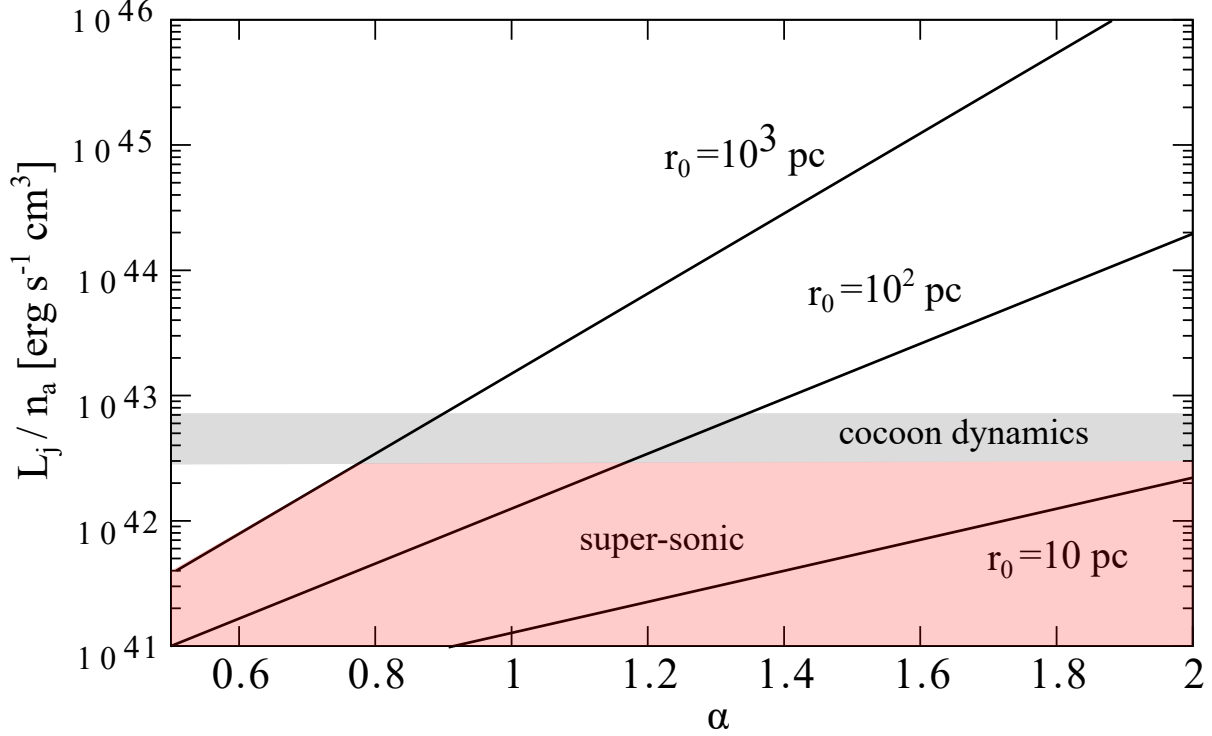


Figure 6. Same as Figure 5, but for the condition of the super-sonic expansion of the inner cocoon with $t_j = 12$ yr and $R_h = 1.4$ pc.

diffuse gas density around the cocoons as seen in Figures 7 and 8. The gray-shaded regions represent the allowed range of $n_a(R_h)$ for two different sizes of cocoons, considering the uncertainty in the inclination angle $\theta = 18^\circ - 65^\circ$ and in the size of cocoon R_h . Note that the uncertainty in the size of the inner cocoon is $R_h = 1.4 - 4$ pc, while that in the size of the outer cocoon is $R_h = 5.6 - 16$ pc. Figure 7 shows that for $r_0 = 10^3$ pc, the number density is $n_a(R_h) = 2 - 20 \text{ cm}^{-3}$ at the head of the inner cocoon, while $n_a(R_h)$ is $10 - 3 \times 10^3 \text{ cm}^{-3}$ at the head of the outer cocoon. For $r_0 = 10^2$ pc, we find that the ambient density of the inner cocoon is $n_a(R_h) = 0.5 - 15 \text{ cm}^{-3}$ and that of $n_a(R_h) = 3 - 30 \text{ cm}^{-3}$ as seen in Figure 8. Thus, Figures 7 and 8 indicate that the median gas density around the inner cocoon is at least one order of magnitude lower than that around the outer cocoon. Regarding the difference in $n_a(R_h)$ around the inner/outer cocoons, we can interpret that the inner cocoon, recently formed by the jet emitted about 10 years ago, is expanding within the low-density cocoon created by the jet emitted about 50 years ago.

It is worth to comparing with previous work on the diffuse gas density at central 10 pc region. Y. Fujita et al. (2016a) estimated the gas density profiles in the innermost regions of 28 nearby FRI/FRII radio galaxies (including 3C 84) with $n_a \simeq 1 - 30 \text{ cm}^{-3}$, assuming that hot gas outside the Bondi radius is in nearly a hydrostatic equilibrium in a gravitational potential, and the gas temperature near the galaxy center is close to the virial temperature of the galaxy. Thus, our results are broadly consistent with the range of the diffuse gas density $n_a(r < 10 \text{ pc})$ estimated at the center of 28 radio galaxies (including 3C84). On the other hand, for the outer cocoon, we show the possibility of a unusual high number density of the ambient gas with $n_a \sim 10^2 - 10^3 \text{ cm}^{-3}$. If this is the case, it would be worth to constraining n_a by using other independent method, e.g., the Farady rotation measurement.

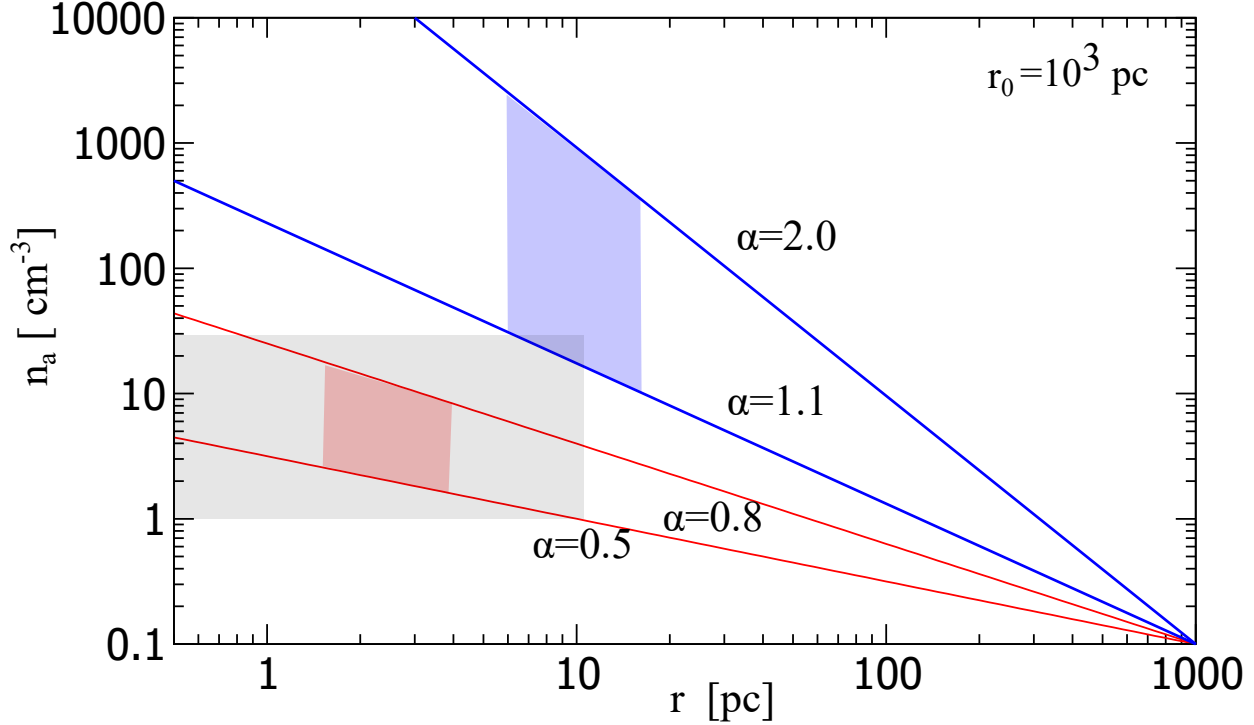


Figure 7. Predicted diffuse gas density around the inner (red lines) and outer cocoon (blue lines) for $r_0 = 10^3$ pc. The red lines corresponds to $\alpha = 0.5 - 0.8$, and the blue lines corresponds to $\alpha = 1.1 - 2.0$, respectively. The red and blue shaded regions represent the allowed range of $n_a(R_h)$ for different size of cocoons, considering the uncertainty of inclination angle $\theta = 18^\circ - 65^\circ$. The gray shaded area denote the diffuse gas density ($r < 10$ pc) at 28 radio galaxies (Y. Fujita et al. 2016a).

3.2. Estimated L_j for inner and outer cocoons

By combining $L_j/n_a(R_h)$ and $n_a(R_h)$, we can finally evaluate the total kinetic power of the jets (L_j) for the inner and outer cocoons. Comparing the jet power for the inner and outer cocoons with the different scales, we discuss the time evolution of $L_j = L_j(t)$. Figure 9 shows the total kinetic power of the inner and outer cocoons for $r_0 = 10^3$ pc. As a result, the total kinetic power of the inner cocoon is $(0.9 - 14) \times 10^{43}$ erg s $^{-1}$, while that of the outer cocoon is $(0.09 - 5.1) \times 10^{46}$ erg s $^{-1}$. We also examine the dependence of r_0 on L_j . For $r_0 = 10^2$ pc, it is found that L_j for the inner cocoon is $(2 - 11) \times 10^{43}$ erg s $^{-1}$ and L_j is $(0.03 - 1.1) \times 10^{46}$ erg s $^{-1}$ for the outer cocoon as seen in Figure 10.

As seen in Figures 9 and 10, we constrain their maximum/minimum jet kinetic power as follows. For the minimum jet power, we adopt the observed Synchrotron emission from the inner cocoon. Taking the minimum energy conditions as the base, T. Savolainen et al. (2023) estimated the lower limit of the inner jet power $L_{j,\min} = 2 \times 10^{43}$ erg s $^{-1}$. Based on this lower jet power, we can constrain the minimum ambient density around the inner cocoon with $n_a(R_h = 1.4 \text{ pc}) \simeq 6 \text{ cm}^{-3}$. On the other hand, we constrain the maximum jet power by the condition in which the inner cocoon is over-pressured. When the inner over-pressured cocoon can evolve in the cavity formed by the outer jets, the pressure of the inner cocoon $P_{c,\text{inner}}$ must be greater than that of the outer cocoon $P_{c,\text{outer}}$. From this condition, the maximum ratio of $L_{j,\text{outer}}/L_{j,\text{inner}}$ is $\simeq 370$.¹ Thus, we find that the upper limit of the outer jet power is $L_{j,\max} \simeq 5 \times 10^{46}$ erg s $^{-1}$. As a result, the jet power of the outer cocoon is $10^{45-46.5}$ erg s $^{-1}$, while that of the inner cocoon is 10^{43-44} erg s $^{-1}$.

¹ The cocoon pressure P_c is obtained as the equation of energy conservation in the cocoon;

$$\frac{\hat{\gamma}}{\hat{\gamma} - 1} \frac{P_c V_c}{t_{\text{age}}} = L_j,$$

where P_c and V_c are the total one-side cocoon pressure and the volume of one-side cocoon, respectively. Here we assume $\hat{\gamma} = 4/3$, since the cocoon is expected to be dominated by relativistic particles for FRIs and 3C84 (e.g., M. C. Begelman & D. F. Cioffi 1989; M. Kino et al. 2007). The volume of the cocoon is measured by $V_c = (4\pi/3)R_h^3$. Thus, the maximal ratio of $L_{j,\text{outer}}/L_{j,\text{inner}}$ is given by

$$\frac{L_{j,\text{outer}}}{L_{j,\text{inner}}} = \left(\frac{t_{\text{age,inner}}}{t_{\text{age,outer}}} \right) \left(\frac{R_{h,\text{outer}}}{R_{h,\text{inner}}} \right)^3 \simeq 370,$$

where $t_{\text{age,inner}} = 12 \text{ yr}$, $t_{\text{age,outer}} = 55 \text{ yr}$, $R_{h,\text{inner}} = 1.4 \text{ pc}$ and $R_{h,\text{outer}} = 16 \text{ pc}$.

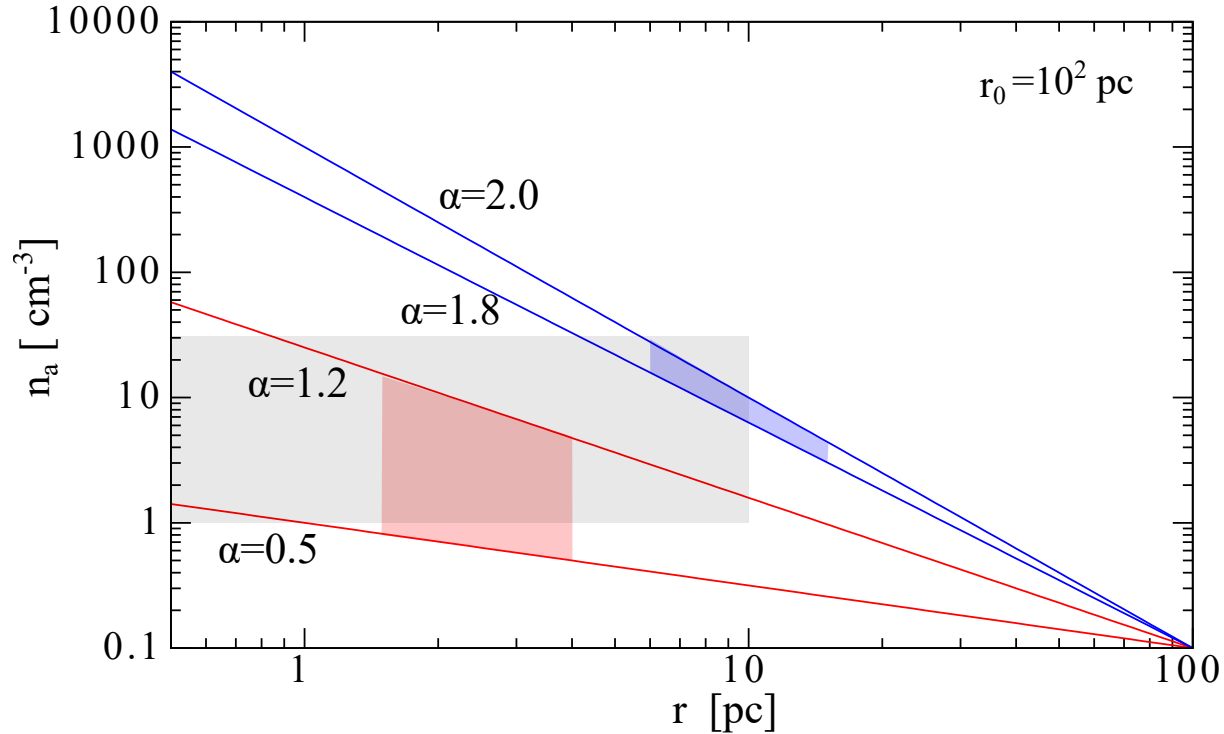


Figure 8. Same as Figure 6, but for $r_0 = 10^2$ pc. The red lines corresponds to $\alpha = 0.5 - 1.2$, and the blue lines corresponds to $\alpha = 1.8 - 2.0$, respectively.

Overall, we find that the total kinetic power of the older outer cocoon is one or two orders of magnitude higher than that of the inner cocoon. That is, the total kinetic power L_j is not constant in time, at least for approximately 50 yr. On the other hand, the observed peak radio flux density of the outer cocoon is 60 Jy at 37 GHz (e.g., N. S. Nesterov et al. 1995), while that of the inner cocoon is 10 Jy at 43 GHz (e.g., K. Suzuki et al. 2012; H. Nagai et al. 2012). In relation to this, the broad $H\beta$ emission line is correlated with the millimeter-wave luminosity of the outer cocoon (B. Punsly et al. 2018). This might indicate that both jet power and accretion power were decreasing. These trends could be roughly consistent with what we found in this paper.

In general, the jet power is related to not only the mass accretion rate onto a SMBH but also the magnetic fields around a SMBH and the BH spin (e.g., M. Zamaninasab et al. 2014). However, for the jetted AGNs (radio-loud AGNs), the jet power is proportional to the accretion luminosity (e.g., S. Rawlings & R. Saunders 1991; G. Ghisellini et al. 2014). In addition, the general relativistic magnetohydrodynamics simulations found that the poloidal magnetic flux ($\Phi_{\text{BH}} \equiv \phi_{\text{BH}} \sqrt{\dot{M}_{\text{acc}} R_s^2 c}$) in the accretion flow is advected inward until the ram pressure of accretion gas is balanced with the magnetic pressure, where ϕ is the dimensionless magnetic flux (e.g., A. Tchekhovskoy et al. 2011; F. Yuan & R. Narayan 2014). If the Blandford and Znajek (BZ) process (R. D. Blandford & R. L. Znajek 1977), where the electromagnetic energy extraction from a rotating BH (\dot{M}_{acc}) is operated as a jet launching mechanism, the jet power is proportional to the mass accretion onto a SMBH because of $\Phi_{\text{BH}} \propto \dot{M}_{\text{BH}}^{0.5}$. Thus, postulating that the relativistic jet is mainly powered by the release of gravitational energy (L_{acc}) of accreting matter, although the jet power is also related to the BH spin, the jet power (L_j) can be proportion to L_{acc} . Thus, L_j/L_{Edd} gives the minimum mass accretion rate normalized by the Eddington mass accretion rate. We here briefly discuss on the efficiency of the jet power (L_j/L_{Edd}) for the inner and outer cocoons in 3C 84. We found that 0.01% – 0.2% of the Eddington luminosity L_{Edd} is carried away as the kinetic power of the inner cocoon, where $L_{\text{Edd}} = 9.6 \times 10^{46} \text{ erg s}^{-1}$ with $M_{\text{BH}} = 8 \times 10^8 M_{\odot}$ (J. Scharwächter et al. 2013). On the other hand, L_j of the outer cocoon is 3% – 40% of L_{Edd} . We here compare with L_j/L_{Edd} of other radio galaxies as shown in Figure 11. It is found that L_j/L_{Edd} of the inner cocoon is similar to that of less powerful FRI radio galaxies (Y. Fujita et al. 2016a) and that of the outer cocoon is comparable with that of powerful FRII radio galaxies (H. Ito et al. 2008). Thus, whether the radio sources are short-lived would be

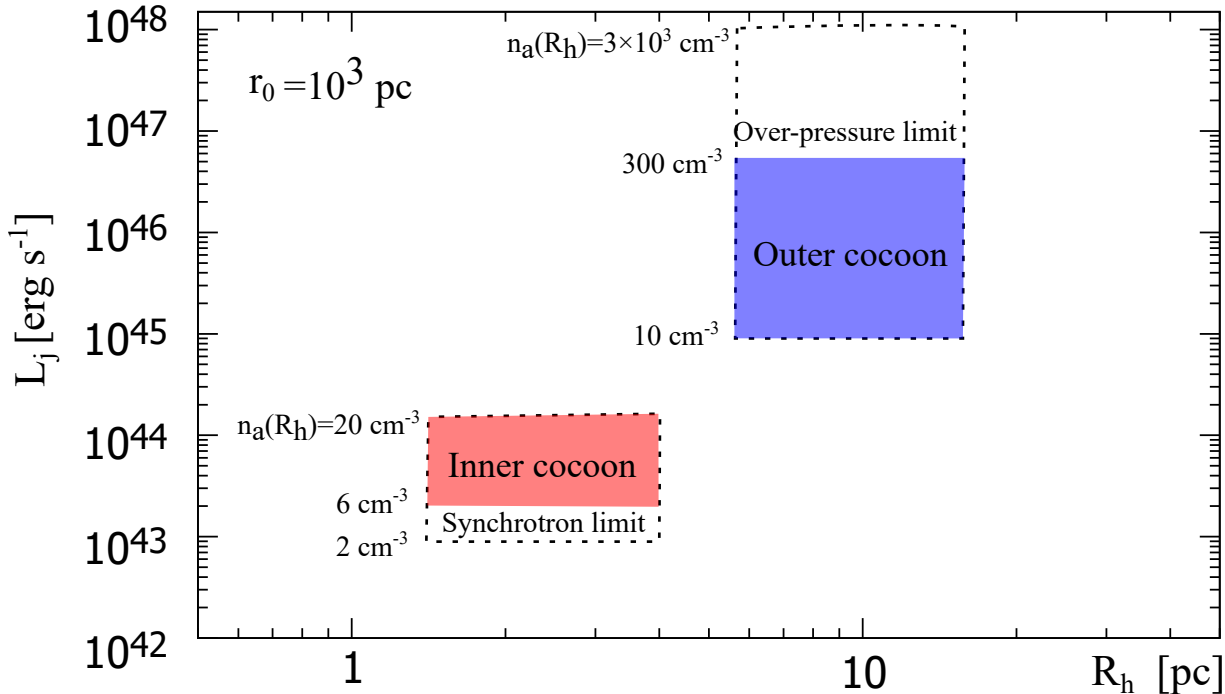


Figure 9. Total kinetic power is function of the distance from the BH for $r_0 = 10^3$ pc. The dotted black square shows the allowed area not including the over-pressure limit and Synchrotron limit. The red region is the average kinetic power of the inner cocoon, while the blue region corresponds to that of outer cocoon. The corresponding ambient density $n_a(R_h)$ is also shown at the left side of allowed regions (red and blue).

independent of M_{BH} and L_j/L_{Edd} . This suggests that the mass accretion may have changed drastically in the last 50 years. In the next section, we will discuss how the accretion can change and the origin of the short-lived outer cocoon with high L_j .

4. DISCUSSIONS

Our analysis in Section 3 indicates that the production of a high-luminosity jet (L_j) over a short period was probably responsible for the generation of the outer cocoon. To achieve this through a change in the accretion rate, a significant and rapid increase in the mass accretion rate would be required, occurring within a brief timescale of a few tens of years to activate the jet. In Section 4.1, we investigate whether the instability of the accretion disk could naturally account for the required L_j within the required timescale of 25-50 years. In Section 4.2, we also consider another possible scenario of tidal disruption events (TDEs) of massive stars as a major source of mass supply (e.g., A. C. S. Readhead et al. 1994; C. Ricci & B. Trakhtenbrot 2023; A. C. S. Readhead et al. 2024). We will discuss these two possibilities as follows.

4.1. Scenario of outer cocoon formation driven by disk instability

One possibly relevant mechanism is thermal instability, associated with changes in the surface density of the disk driven by changes in opacity (e.g., D. N. C. Lin & G. A. Shields 1986; B. Czerny et al. 2009). The state transitions expected for these disk instabilities happen at an Eddington ratio of a few percent, which is observed in some AGNs and black hole binaries (e.g., A. C. S. Readhead et al. 1994; T. An & W. A. Baan 2012; C. Ricci & B. Trakhtenbrot 2023; A. C. S. Readhead et al. 2024). To check if the disk instability is valid for the outer cocoon in 3C 84, we examine relevant key physical quantities, i.e., dynamical timescale (t_{dyn}), viscous timescale (t_{vis}), thermal timescale (t_{th}), accretion power (L_{acc}) and jet power (L_j). First, we discuss these timescales for the outer cocoon, assuming the standard accretion disk. In general, the variability in time may be caused by the motion of the gas with circular velocity v_c within the

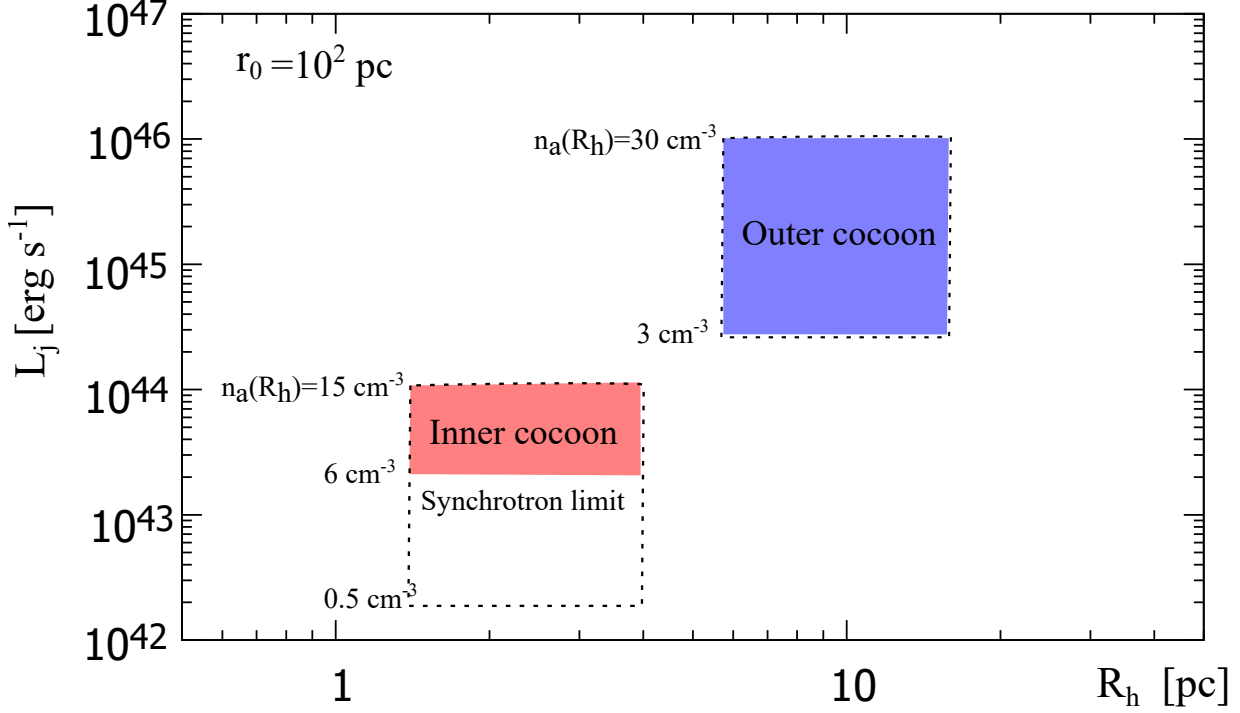


Figure 10. Same as Figure 8, but for $r_0 = 10^2$ pc.

accretion disk, whose size is R_{AD} . The dynamical timescale is determined by

$$t_{\text{dyn}} = \frac{R_{\text{AD}}}{v_c} \simeq 0.3 \text{ yr} \left(\frac{R_{\text{AD}}}{150 R_s} \right)^{3/2} \left(\frac{M_{\text{BH}}}{10^9 M_\odot} \right), \quad (12)$$

where R_s is the Schwarzschild radius, $R_s = 2GM_{\text{BH}}/c^2$. We here adopt $R_{\text{AD}} = 150 R_s$ as a fiducial value for the UV-emitting disk size, i.e., the typical outer radius of the accretion disk, assuming a standard thin disk model (e.g., S. Kato et al. 2008). The timescale associated with the disk heating up or cooling down, i.e. the thermal timescale, can be estimated as

$$t_{\text{th}} \simeq \frac{t_{\text{dyn}}}{\alpha} \simeq 10 \text{ yr} \left(\frac{\alpha_{\text{vis}}}{0.03} \right)^{-1} \left(\frac{R_{\text{AD}}}{150 R_s} \right)^{3/2} \left(\frac{M_{\text{BH}}}{10^9 M_\odot} \right). \quad (13)$$

On the other hand, by analogy to black hole X-ray binaries, the variability may be driven by the high-to-soft state transitions (e.g., H. Noda & C. Done 2018; J. J. Ruan et al. 2019). The timescale of these transitions can be comparable to the viscous timescale (B. Czerny et al. 2009)

$$t_{\text{vis}} \simeq 5 \times 10^3 \text{ yr} \left(\frac{H_{\text{AD}}/R_{\text{AD}}}{0.05} \right)^{-2} \left(\frac{\alpha_{\text{vis}}}{0.03} \right)^{-1} \left(\frac{R_{\text{AD}}}{150 R_s} \right)^{3/2} \left(\frac{M_{\text{BH}}}{10^9 M_\odot} \right), \quad (14)$$

where H_{AD} and α_{vis} are the scale height and the viscous parameter of the accretion disk (N. I. Shakura & R. A. Sunyaev 1973; S. Kato et al. 2008). We use $\alpha_{\text{vis}} = 0.03$ as a fiducial value because the numerical simulations derive the estimation of $\alpha_{\text{vis}} \sim 0.03$ (e.g., M. Machida et al. 2000; M. Machida & R. Matsumoto 2003; S. Hirose et al. 2009; S. W. Davis et al. 2010). For a standard thin disk, the disk aspect ratio ($H_{\text{AD}}/r_{\text{AD}}$) is typically very small, and we assume $H_{\text{AD}}/R_{\text{AD}} = 0.05$ by following D. Stern et al. (2018). Thus, it is found that t_{age} is longer than t_{dyn} and shorter than t_{vis} and roughly comparable to t_{age} . Note that increasing the aspect ratio, $H_{\text{AD}}/R_{\text{AD}}$ leads to shorter viscous timescales (Eq.(14))(e.g., C. Ricci & B. Trakhtenbrot 2023). Therefore, in terms of the timescales, the age of the outer cocoon may be explained by these disk instabilities. Moreover, we should mention that the timescale of fast

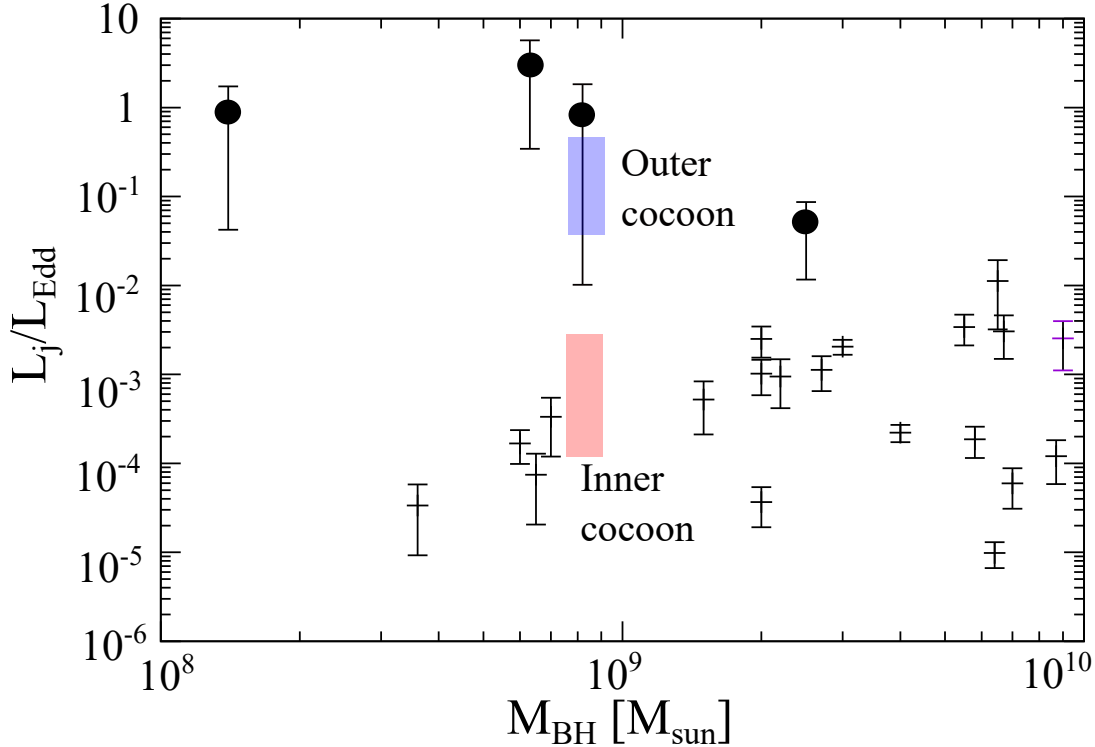


Figure 11. Jet efficiency L_j/L_{Edd} against the BH mass M_{BH} . The red region is the allowed kinetic energy of the inner cocoon and the blue region corresponds to that of outer cocoon. The black crosses denote the FRI radio galaxies (Y. Fujita et al. 2016a), and the black circles show the powerful FRII radio galaxies (H. Ito et al. 2008).

radio variations occurred in 1959, i.e., a few years, is similar to t_{dyn} . This might indicate that the mass accretion rate increases drastically caused by the disk instability.

Next we compare the jet power with the accretion power. As we already mentioned in § 3.2, we here suppose that the accretion disk has a radiative luminosity of $L_{\text{acc}} = \epsilon \dot{M}_{\text{acc}} c^2$, where \dot{M}_{acc} and ϵ are the mass accretion rate and the radiative efficiency $\epsilon \sim 0.05 - 0.4$ (e.g., N. I. Shakura & R. A. Sunyaev 1973; S. A. Balbus & J. F. Hawley 1991). On the other hand, the jet power is expressed as $L_{\text{jet}} = \eta \dot{M}_{\text{acc}} c^2$ where $\eta = 0.1 - 3$. Especially, η reaches maximally $\eta_{\text{max}} \sim 3$ for the magnetically arrested accretion (MAD) phase with the BH spin (e.g., A. Tchekhovskoy et al. 2011; R. Narayan et al. 2022). Thus, a near-maximally rotating BH put roughly 10 times as much power into jets as could be released by the accreted in a steady radiatively efficient flow, i.e.,

$$L_j = \left(\frac{\eta}{\epsilon}\right) L_{\text{acc}} \simeq 10 L_{\text{acc}}, \quad (15)$$

where $\eta \sim 3$ and $\epsilon \sim 0.4$. This may be a proper upper limit, since the jet power in blazar is maximally 10 times greater than the luminosity of their accretion disks (e.g., G. Ghisellini et al. 2014). Thus, the expected maximum jet power L_j , which is derived from the observed mass accretion disk luminosity in 3C 84 with $L_{\text{acc}} = 4 \times 10^{44} \text{ erg s}^{-1}$ (A. Levinson et al. 1995), is obtained as

$$L_{j,\text{max}} \simeq 4 \times 10^{45} \text{ erg s}^{-1}. \quad (16)$$

This value is one order of magnitude lower than the upper value of jet power with $L_j \simeq (1 - 5) \times 10^{46} \text{ erg s}^{-1}$ (see Figures 9 and 10). This may suggest the extremely high accretion rate, which is one order magnitude higher than the mass accretion rate in the persistent state ($\dot{M}_{\text{acc}} \simeq 6 \times 10^{-2} M_{\odot} \text{ yr}^{-1}$), happened about 25 – 50 years ago driven by the disk instability, in order to explain the formation of outer cocoon, where $\dot{M}_{\text{acc}} = L_{\text{acc}}/(\epsilon c^2)$ with $\epsilon = 0.1$.

4.2. Scenario of outer cocoon formation driven by tidal disruption events of stars

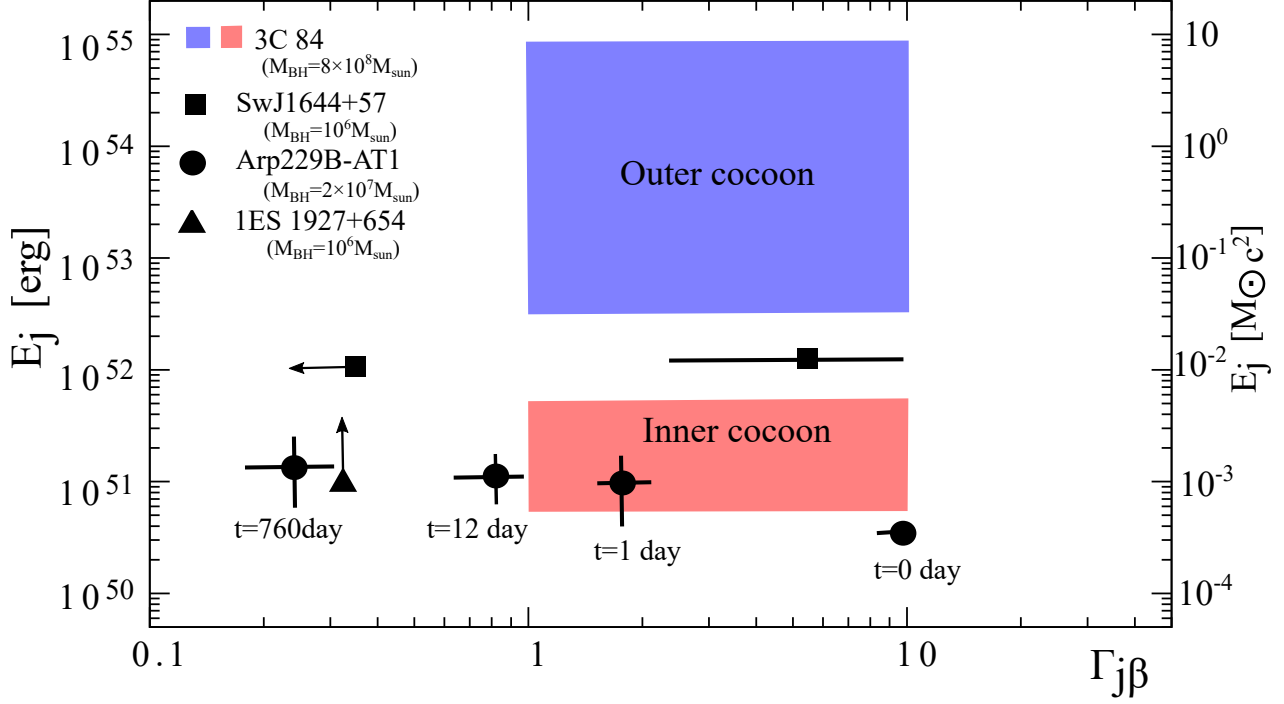


Figure 12. Jet kinetic energy E_j versus the expansion speed $\Gamma_j\beta$, where $\Gamma_j = (1 - \beta^2)^{-1/2}$ is the bulk Lorentz factor and $\beta = v/c$. The red and blue regions denote the case of 3C 84 jets ($M_{\text{BH}} = 8 \times 10^8 M_\odot$). The red region is the allowed kinetic energy of the inner cocoon and the blue region corresponds to that of outer cocoon with $\Gamma_j\beta = 1 - 10$ (G. Giovannini et al. 2018). The right vertical axis denotes the jet kinetic energy in unit of $M_\odot c^2$. The black square show SwJ1644+57 ($M_{\text{BH}} \simeq 10^6 M_\odot$) (B. A. Zauderer et al. 2011), the black circle denotes Arp298-B AT1 ($M_{\text{BH}} \simeq 2 \times 10^7 M_\odot$) for four different epochs, i.e., from right to left, just after the jet is launched, one day, 12 days and 760 days (S. Mattila et al. 2018), and the black triangle is the upper limit of E_j for 1ES 1927 + 654 ($M_{\text{BH}} \simeq 10^6 M_\odot$), assuming $L_j = 10^{43} \text{ erg s}^{-1}$, $t_{\text{age}} = 3 \text{ yr}$ and $\beta = 0.3$ (E. T. Meyer et al. 2024). The arrow is the upper limit for the expansion speed of SwJ1644+57 (J. Yang et al. 2016).

In this sub-section, we propose a novel scenario of TDE of a star as a source of mass supply within the short period for the outer cocoon of 3C84. Some AGN jets are indeed to be suggested to be powered by TDEs, whose light curves are characterized by a power-law decay with an index of $-5/3$. So far, several candidate jets/outflows from TDEs have been observed. For two Swift sources (SwJ1644+57, SwJ2058+05), sudden switch-on and switch-off over a period of two years indicated that jet launching could be associated with super-Eddington accretion (J. S. Bloom et al. 2011; D. N. Burrows et al. 2011).

Recently, S. Mattila et al. (2018) discovered the spatially resolved relativistic jet structure associated with a bright infrared flare such as Arp299B-AT1 in the nucleus of the Arp 299 galaxy. Recently, multi-wavelength observations support the interpretation of AT2022cmc as a jetted TDE containing a synchrotron afterglow, likely launched by a SMBH with spin (I. Andreoni et al. 2022). Moreover, the destruction and recreation of the X-ray corona could occur by the TDE like a changing look AGN 1ES 1927 + 654 (C. Ricci et al. 2020). Interestingly, this object has recently shown a newly launched radio jet a few years after the destruction of the X-ray corona (E. T. Meyer et al. 2024). Theoretically, this may be explained by the rapid increase in the mass accretion rate due to the shocks between the accretion disk and the stellar debris (e.g., C.-H. Chan et al. 2019).

Statistically, the birth rate of jetted TDEs with $0.02 - 10^3 \text{ Gpc}^{-3} \text{ yr}^{-1}$ (e.g., D. N. Burrows et al. 2011; F. De Colle & W. Lu 2020; I. Andreoni et al. 2022) is much higher than the birth rate of compact symmetric objects (CSOs) with $\sim 3 \times 10^{-5} \text{ Gpc}^{-3} \text{ yr}^{-1}$ (A. C. S. Readhead et al. 2024), although the intrinsic fraction of jet-accompanying events is largely unconstrained in the range of 0.001% – 34% (T. Kawamuro et al. 2016). Considering the evidence that most CSOs are short-lived AGNs (S. Kiehlmann et al. 2024a; A. C. S. Readhead et al. 2024), some CSOs would be linked to TDEs.

Here we discuss the possibility that the properties of the outer cocoon in 3C 84 are explained by TDEs in terms of the timescale and the total jet energy.

Generally, TDEs occur when stars pass within the tidal radius R_T at the pericenter of their orbit around an SMBH where R_T is determined by the balance between the self-gravity of stars and the tidal force of the SMBH, i.e., $GM_*/R_*^3 \simeq (GM_{\text{BH}}/R_T^2) \times (R_*/R_T)$. The ratio of R_T to R_s is

$$\frac{R_T}{R_s} \simeq 1.6 \left(\frac{M_*}{3M_\odot} \right)^{-1/3} \left(\frac{R_*}{10R_\odot} \right) \left(\frac{M_{\text{BH}}}{10^9 M_\odot} \right)^{-2/3}, \quad (17)$$

where M_* and R_* are the mass and radius of each star undergoing tidal disruption (e.g., [M. MacLeod et al. 2012](#)). Thus, only massive stars ($M_* > 3M_\odot$) and/or post-main sequence stars can be observably disrupted by SMBHs with $M_{\text{BH}} \sim 10^9 M_\odot$ in 3C 84 (e.g., [A. C. S. Readhead et al. 2024](#)). Recently, [J. Lim et al. \(2020\)](#) reported thousands of compact and massive blue star clusters have formed at a steady rate over past 1 Gyr around 3C 84. This might support that some massive stars in these star clusters is a major source of mass supply.

During the encounter, material is stripped from the stellar core and spread into two tidal tails. The material in one of the tails is unbound from the black hole and ejected on hyperbolic trajectories. The other is bound to the black hole and returns on a wide range of elliptical orbits. Following [M. J. Rees \(1988\)](#), we can evaluate the fallback time of the most bound material t_{fb} , assuming that the star is initially on a parabolic orbit. The characteristic timescale on which post-TDE bound material falls back onto the SMBH is the fallback timescale, t_{fb} as

$$t_{\text{fb}} \simeq 40 \text{ yr} \left(\frac{M_*}{3M_\odot} \right)^{-1} \left(\frac{R_*}{10R_\odot} \right)^{3/2} \left(\frac{M_{\text{BH}}}{10^9 M_\odot} \right)^{1/2}. \quad (18)$$

Thus, the TDE timescale is $t_{\text{TDE}} \simeq t_{\text{fb}} \sim 40 \text{ yr}$, which is roughly comparable to the age of the short-lived outer cocoon $t_{\text{age}} = 50 \text{ yr}$. On the other hand, t_{fb} is much longer than the duration of the rapid flare phenomena in the optical band, i.e., several months ([N. S. Nesterov et al. 1995](#)). Thus, such the short timescale variability may not be related to TDEs phenomena (e.g., [I. Andreoni et al. 2022](#)) but the AGN intrinsic phenomena such as disk instability.

Next, the maximal accretion rate can be estimated as the ratio M_*/t_{fb} ,

$$\dot{M}_{\text{max}} = \frac{M_*}{t_{\text{fb}}} \simeq 0.1 M_\odot \text{ yr}^{-1} \left(\frac{M_*}{3M_\odot} \right)^2 \left(\frac{R_*}{10R_\odot} \right)^{-3/2} \left(\frac{M_{\text{BH}}}{10^9 M_\odot} \right)^{-1/2}. \quad (19)$$

The expected maximum jet power associated with TDE, $L_{j,\text{max}} = \eta \dot{M}_{\text{max}} c^2$ is given by

$$L_{j,\text{max}} \simeq 2 \times 10^{46} \text{ erg s}^{-1} \left(\frac{M_*}{3M_\odot} \right)^2 \left(\frac{R_*}{10R_\odot} \right)^{-3/2} \left(\frac{M_{\text{BH}}}{10^9 M_\odot} \right)^{-1/2}, \quad (20)$$

where we adopt $\eta = 3$ as an upper value for the MAD phase with the BH spin. This value is comparable to the maximal jet power of the outer cocoon. Moreover, the maximum energy E_j deposited within the outer cocoon during t_{age} is

$$E_j \simeq 1.5 \times 10^{54} \text{ erg} \left(\frac{L_j}{10^{46} \text{ erg/s}} \right) \left(\frac{t_{\text{age}}}{50 \text{ yr}} \right). \quad (21)$$

Taking into account the uncertainty of E_j , Figure 12 shows that the allowed range of E_j corresponds to $3 \times 10^{-2} - 10 M_\odot c^2$. Thus, the total energy embedded in the outer cocoon may be explained by a single massive star capture by a SMBH. As seen in Figure 12, we found that the kinetic energy of the outer cocoon is relatively higher than that of three jetted TDEs such as "SwJ 1644+57" ($M_{\text{BH}} \simeq 10^6 M_\odot$) ([B. A. Zauderer et al. 2011](#)), "Arp299B-AT1" ($M_{\text{BH}} \simeq 2 \times 10^7 M_\odot$) ([S. Mattila et al. 2018](#)) and 1ES1927 +654 ($M_{\text{BH}} \simeq 10^6 M_\odot$) ([E. T. Meyer et al. 2024](#)) which show a prominent extended jet structure and a rapid decrease in radio luminosity over a few years. The SMBH mass of 3C 84 is two-three orders of magnitude larger, and thus the short-lived jet in 3C84 may be a scale-up version of jetted TDEs because of $E_j \propto M_{\text{BH}}$. Table 2 summarizes the comparison of the properties of the outer cocoon with two possible scenarios. From these, the formation of outer cocoon associated with the extreme accretion events may be driven by the tidal disruption events (TDEs) of massive stars and/or the disk instability.

Table 2. Comparison of the properties of the outer cocoon with two scenarios

	Outer cocoon	Disk instability	TDE	
Timescale of variability	$t_{\text{age}} \sim 50 \text{ yr}$	$t_{\text{dyn}} \sim 0.3 \text{ yr}, t_{\text{th}} \sim 10 \text{ yr}$	$t_{\text{vis}} \sim 10^4 \text{ yr}$	$t_{\text{fb}} \sim 40 \text{ yr}$
Maximum jet power ($L_{j,\text{max}}$)	$(1 - 5) \times 10^{46} \text{ erg s}^{-1}$	$\sim 5 \times 10^{45} \text{ erg s}^{-1}$		$\sim 2 \times 10^{46} \text{ erg s}^{-1}$
Total deposited energy (E_j)	$\sim 1.5 \times 10^{54} \text{ erg}$	–		$\sim 10^{54} \text{ erg} (\simeq M_{\odot} c^2)$

Based on the TDE scenario, we next discuss the evolutionary sequence of the inner and outer cocoons in 3C 84 as seen in Figure 13. phase (a): In the early life of the outer cocoon, their edge-brightened lobes (gray-colored bubbles) with prominent hot spots (red-colored circles) are formed by relativistic jets (blue-colored triangles) driven by the stellar TDEs. phase (b): After the jet activity for the outer cocoon is terminated, the outer cocoon must transition from relativistic to subsonic. phase (c): In the late life of the outer cocoon, their expansion is likely subsonic because the apparent motion is not visible and the radio morphology is highly patchy (see also Figure 2). During the late-life of the outer cocoon, the newborn jets propagate within the region of the old, outer cocoon whose density is lower than the ambient gas density around the outer cocoon. This idea is supported by analytical cocoon dynamics and simulations (e.g., C. R. Kaiser et al. 2000; M. Kino et al. 2007).

Observationally, an edge-brightened high luminosity class CSO named CSO 2 is roughly distributed into three subclasses: CSO 2.0s, CSO 2.1s, and CSO 2.2s. CSO 2.0s have prominent hot spots at the leading edges of narrow lobes, while CSO 2.2s have no hot spots and wider lobes. The size and radio luminosity of CSO 2.0s are smaller and larger than CSO 2.2s. In addition, the expansion velocity of CSO 2.0s is $\sim 0.3 c$ (super-sonic), while that of CSO 2.2s is almost negligibly small (sub-sonic). CSO 2.1s represents a hybrid feature between CSO 2.0s and CSO 2.2s. Based on this evidence, an evolutionary sequence CSO 2.0s (phase(a)) \rightarrow CSO 2.1s (phase(b)) \rightarrow CSO 2.2s (phase(c)) has been proposed (A. C. S. Readhead et al. 2024; A. G. Sullivan et al. 2024). Considering the total energy of the outer cocoon ($\sim 10^{54} \text{ erg}$) and the three epochs of the actual 3C 84 images (the fading radio lobes in Figure 2), the physical properties of the outer cocoon resemble the evolutionary sequence of short-lived CSO 2s. Based on the above definition of CSO subclasses, the inner cocoon can also be identified as the new CSO 2.0. Unlike the outer cocoon, the inner cocoon would be in a persistent phase because its jet power $L_j = 10^{43-44} \text{ erg s}^{-1}$ is comparable to the average jet power in the past ($\sim 10^7 \text{ yr}$) estimated by 10 kpc-scale X-ray cavity, e.g. $L_j \simeq 1.5 \times 10^{44} \text{ erg s}^{-1}$ (D. A. Rafferty et al. 2006).

Recently, for TXS 0128 + 554 that are members of CSOs, M. L. Lister et al. (2020) discovered the lack of compact, inverted spectrum hot spots and an emission gap between the bright inner jet and the outer radio lobe structure. This might indicate that the jets have undergone episodic activity and were relaunched a decade ago, which is similar to the properties of the inner and outer cocoons in 3C 84. Therefore, future VLBI monitoring observations for the inner cocoon in 3C 84 and TXS 0128+554 would be one of the crucial methods to explore the origin and formation of CSO 2.0.

5. SUMMARY

We investigated the jet power and the density of ambient matter in the radio jet 3C 84 by using the momentum balance along the jet axis and the transonic condition for the mini-cocoons observed at two different scales (approximately 1 and 6 parsec scales). Our findings are as follows.

1. We precisely determined the ratio of jet power to ambient density, L_j/n_a , to be $(0.3 - 0.7) \times 10^{43} \text{ erg s}^{-1} \text{ cm}^3$ for the inner cocoon. Similarly, for the outer cocoon, we found that this value is more than an order of magnitude larger at $(0.9 - 3.7) \times 10^{44} \text{ erg s}^{-1}, \text{ cm}^3$. This indicates that the outer cocoon is formed by a powerful jet that propagates through an ambient gas density of $n_a = 20 - 300 \text{ cm}^{-3}$, with a jet power of $10^{45-46.5} \text{ erg s}^{-1}$. On the other hand, the inner cocoon is formed by a weaker jet with a power of $10^{43-44} \text{ erg s}^{-1}$, propagating through a relatively low-density environment of $n_a = 6 - 20 \text{ cm}^{-3}$. Regarding the difference in ambient gas density n_a , it appears to support the hypothesis that the inner cocoon, recently formed about 10 years ago, is expanding within the low-density cocoon created by the jet emitted about 50 years ago.

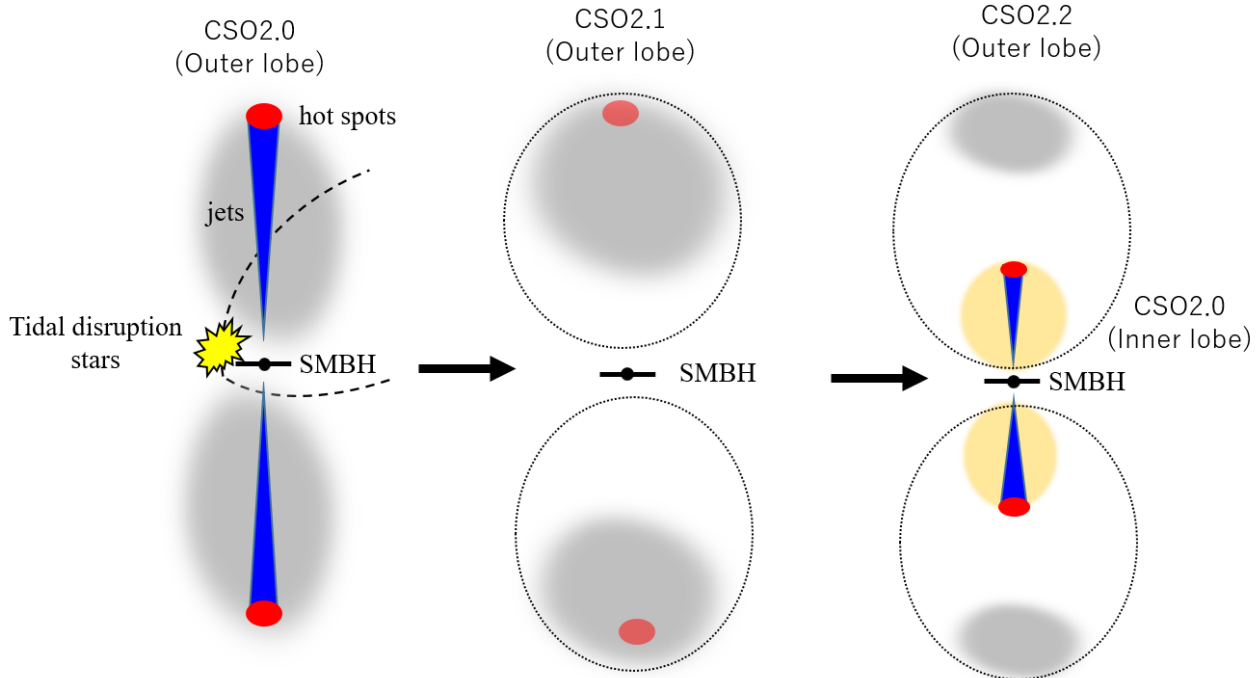


Figure 13. A diagram of the evolutionary sequence of inner (~ 1 pc) and outer (6 pc) cocoon in 3C 84 based on the recently proposed evolution model of CSO2 powered by the TDEs (A. G. Sullivan et al. 2024). In the early-life of outer cocoon (CSO 2.0s), their edge-brightened lobes (gray-colored bubbles) with prominent hot spots (red-colored circles) are formed by a relativistic jets (blue-colored triangles) driven by the interaction between the tidal disruption stars and accretion disk. As the bound gas mass is exhausted (or the accretion disk is destroyed by the interaction), the jet activity for the outer cocoon must be terminated. After that the outer cocoon transits from the super-sonic expansion to sub-sonic one. This phase corresponds to the mid-life of CSO 2s, namely CSO 2.1. In the late-life of outer cocoon (CSO 2.2s), their expansion is likely subsonic because the apparent motion is invisible and the radio morphology is highly patchy (see also Figure 2). During the late-life of outer cocoon, the new born jets propagate within it, and thus the inner cocoon (small orange-colored bubbles) would be identified as the new CSO 2.0.

2. We found that the jet efficiency (L_j/L_{Edd}) rapidly decreases from 3 – 40% (outer cocoon) to 0.01 – 0.2% (inner cocoon) over $\simeq 50$ yr. To explain the short-lived outer cocoon with high L_j , a significant mass accretion, i.e., $\geq 10\%$ of the Eddington mass accretion rate, must be required over a short period (~ 50 yr) to activate the jet. This may suggest the extremely high accretion rate driven by disk instability, which is one order magnitude higher than the averaged mass accretion rate, happened about 25 – 50 years ago. Alternatively, the maximum energy E_j embedded within the outer cocoon during $t_{\text{age}} \sim 50$ yr corresponds to $3 \times 10^{-2} - 10 M_{\odot} c^2$. Thus, the total energy embedded in the outer cocoon may be explained by massive stars and/or post main sequence stars captured by a SMBH.
3. Following CSO evolutionary scenario proposed by A. G. Sullivan et al. (2024), we discuss the evolutionary sequence of the inner and outer cocoons in 3C 84 as follows: (i) In the early life of the outer cocoon (CSO 2.0s), their edge-brightened lobes with prominent hot spots are formed by relativistic jets driven by TDE of stars. (ii) After the jet activity for the outer cocoon is terminated in about 50 years, the outer cocoon must transition from relativistic to subsonic. This phase corresponds to the mid-life of CSO 2s, namely CSO 2.1. (iii) In the late life of the outer cocoon (CSO 2.2s), their expansion is likely subsonic because the apparent motion is visible and the radio morphology is highly patchy. During the late life of the outer cocoon, the newly born inner jets can propagate within the region of the old, outer cocoon whose density is lower than the ambient gas density around the outer cocoon. Thus, the inner cocoon could be identified as the new CSO 2.0.

ACKNOWLEDGMENTS

We thank the referee for his/her careful read of this manuscript and valuable comments. The authors thank K. Ohsuga, H. Nagai, S. Yoshioka for their valuable comments to the discussions. This research used data from the MOJAVE database that is maintained by the MOJAVE team (M. L. Lister et al. 2018). This study was supported by JSPS KAKENHI grant Nos. 19K03918 (NK), JP22H00157 (MK), and 21H04496 (KW).

REFERENCES

- Alexander, P. 2000, Evolutionary models for radio sources from compact sources to classical doubles, *MNRAS*, 319, 8, doi: [10.1046/j.1365-8711.2000.03711.x](https://doi.org/10.1046/j.1365-8711.2000.03711.x)
- An, T., & Baan, W. A. 2012, The Dynamic Evolution of Young Extragalactic Radio Sources, *ApJ*, 760, 77, doi: [10.1088/0004-637X/760/1/77](https://doi.org/10.1088/0004-637X/760/1/77)
- Andreoni, I., Coughlin, M. W., Perley, D. A., et al. 2022, A very luminous jet from the disruption of a star by a massive black hole, *Nature*, 612, 430, doi: [10.1038/s41586-022-05465-8](https://doi.org/10.1038/s41586-022-05465-8)
- Asada, K., Kamenno, S., Shen, Z.-Q., et al. 2006, The Expanding Radio Lobe of 3C 84 Revealed by VSOP Observations, *PASJ*, 58, 261, doi: [10.1093/pasj/58.2.261](https://doi.org/10.1093/pasj/58.2.261)
- Balbus, S. A., & Hawley, J. F. 1991, A Powerful Local Shear Instability in Weakly Magnetized Disks. I. Linear Analysis, *ApJ*, 376, 214, doi: [10.1086/170270](https://doi.org/10.1086/170270)
- Barai, P., Proga, D., & Nagamine, K. 2012, Multiphase, non-spherical gas accretion on to a black hole, *MNRAS*, 424, 728, doi: [10.1111/j.1365-2966.2012.21260.x](https://doi.org/10.1111/j.1365-2966.2012.21260.x)
- Baum, S. A., & Heckman, T. 1989, Extended Optical Line Emitting Gas in Powerful Radio Galaxies: Statistical Properties and Physical Conditions, *ApJ*, 336, 681, doi: [10.1086/167043](https://doi.org/10.1086/167043)
- Begelman, M. C., Blandford, R. D., & Rees, M. J. 1984, Theory of extragalactic radio sources, *Reviews of Modern Physics*, 56, 255, doi: [10.1103/RevModPhys.56.255](https://doi.org/10.1103/RevModPhys.56.255)
- Begelman, M. C., & Cioffi, D. F. 1989, Overpressured Cocoon in Extragalactic Radio Sources, *ApJL*, 345, L21, doi: [10.1086/185542](https://doi.org/10.1086/185542)
- Bettoni, D., Falomo, R., Fasano, G., & Govoni, F. 2003, The black hole mass of low redshift radiogalaxies, *A&A*, 399, 869, doi: [10.1051/0004-6361:20021869](https://doi.org/10.1051/0004-6361:20021869)
- Birzan, L., Rafferty, D. A., McNamara, B. R., Wise, M. W., & Nulsen, P. E. J. 2004, A Systematic Study of Radio-induced X-Ray Cavities in Clusters, Groups, and Galaxies, *ApJ*, 607, 800, doi: [10.1086/383519](https://doi.org/10.1086/383519)
- Blandford, R. D., & Begelman, M. C. 1999, On the fate of gas accreting at a low rate on to a black hole, *MNRAS*, 303, L1, doi: [10.1046/j.1365-8711.1999.02358.x](https://doi.org/10.1046/j.1365-8711.1999.02358.x)
- Blandford, R. D., & Znajek, R. L. 1977, Electromagnetic extraction of energy from Kerr black holes., *MNRAS*, 179, 433, doi: [10.1093/mnras/179.3.433](https://doi.org/10.1093/mnras/179.3.433)
- Bloom, J. S., Giannios, D., Metzger, B. D., et al. 2011, A Possible Relativistic Jetted Outburst from a Massive Black Hole Fed by a Tidally Disrupted Star, *Science*, 333, 203, doi: [10.1126/science.1207150](https://doi.org/10.1126/science.1207150)
- Burrows, D. N., Kennea, J. A., Ghisellini, G., et al. 2011, Relativistic jet activity from the tidal disruption of a star by a massive black hole, *Nature*, 476, 421, doi: [10.1038/nature10374](https://doi.org/10.1038/nature10374)
- Chan, C.-H., Piran, T., Krolik, J. H., & Saban, D. 2019, Tidal Disruption Events in Active Galactic Nuclei, *ApJ*, 881, 113, doi: [10.3847/1538-4357/ab2b40](https://doi.org/10.3847/1538-4357/ab2b40)
- Choi, J.-H., Shlosman, I., & Begelman, M. C. 2013, Supermassive Black Hole Formation at High Redshifts via Direct Collapse: Physical Processes in the Early Stage, *ApJ*, 774, 149, doi: [10.1088/0004-637X/774/2/149](https://doi.org/10.1088/0004-637X/774/2/149)
- Choi, J.-H., Shlosman, I., & Begelman, M. C. 2015, Supermassive black hole formation at high redshifts via direct collapse in a cosmological context, *MNRAS*, 450, 4411, doi: [10.1093/mnras/stv694](https://doi.org/10.1093/mnras/stv694)
- Czerny, B., Siemiginowska, A., Janiuk, A., Nikiel-Wroczyński, B., & Stawarz, L. 2009, Accretion Disk Model of Short-Timescale Intermittent Activity in Young Radio Sources, *ApJ*, 698, 840, doi: [10.1088/0004-637X/698/1/840](https://doi.org/10.1088/0004-637X/698/1/840)
- Davis, S. W., Stone, J. M., & Pessah, M. E. 2010, Sustained Magnetorotational Turbulence in Local Simulations of Stratified Disks with Zero Net Magnetic Flux, *ApJ*, 713, 52, doi: [10.1088/0004-637X/713/1/52](https://doi.org/10.1088/0004-637X/713/1/52)
- De Colle, F., & Lu, W. 2020, Jets from Tidal Disruption Events, *NewAR*, 89, 101538, doi: [10.1016/j.newar.2020.101538](https://doi.org/10.1016/j.newar.2020.101538)
- Fabian, A. C., Sanders, J. S., Taylor, G. B., et al. 2006, A very deep Chandra observation of the Perseus cluster: shocks, ripples and conduction, *MNRAS*, 366, 417, doi: [10.1111/j.1365-2966.2005.09896.x](https://doi.org/10.1111/j.1365-2966.2005.09896.x)
- Fanti, C., Fanti, R., Dallacasa, D., et al. 1995, Are compact steep-spectrum sources young?, *A&A*, 302, 317

- Fender, R. P., Belloni, T. M., & Gallo, E. 2004, Towards a unified model for black hole X-ray binary jets, *MNRAS*, 355, 1105, doi: [10.1111/j.1365-2966.2004.08384.x](https://doi.org/10.1111/j.1365-2966.2004.08384.x)
- Fujita, Y., Kawakatu, N., & Shlosman, I. 2016a, AGN jet power, formation of X-ray cavities, and FR I/II dichotomy in galaxy clusters, *PASJ*, 68, 26, doi: [10.1093/pasj/psw012](https://doi.org/10.1093/pasj/psw012)
- Fujita, Y., Kawakatu, N., Shlosman, I., & Ito, H. 2016b, The young radio lobe of 3C 84: inferred gas properties in the central 10 pc, *MNRAS*, 455, 2289, doi: [10.1093/mnras/stv2481](https://doi.org/10.1093/mnras/stv2481)
- Fujita, Y., & Nagai, H. 2017, Discovery of a new subparsec counterjet in NGC 1275: the inclination angle and the environment, *MNRAS*, 465, L94, doi: [10.1093/mnrasl/slz217](https://doi.org/10.1093/mnrasl/slz217)
- Gaspari, M., Ruszkowski, M., & Sharma, P. 2012, Cause and Effect of Feedback: Multiphase Gas in Cluster Cores Heated by AGN Jets, *ApJ*, 746, 94, doi: [10.1088/0004-637X/746/1/94](https://doi.org/10.1088/0004-637X/746/1/94)
- Ghisellini, G., Tavecchio, F., Maraschi, L., Celotti, A., & Sbarbato, T. 2014, The power of relativistic jets is larger than the luminosity of their accretion disks, *Nature*, 515, 376, doi: [10.1038/nature13856](https://doi.org/10.1038/nature13856)
- Giovannini, G., Savolainen, T., Orienti, M., et al. 2018, A wide and collimated radio jet in 3C84 on the scale of a few hundred gravitational radii, *Nature Astronomy*, 2, 472, doi: [10.1038/s41550-018-0431-2](https://doi.org/10.1038/s41550-018-0431-2)
- Gugliucci, N. E., Taylor, G. B., Peck, A. B., & Giroletti, M. 2005, Dating COINS: Kinematic Ages for Compact Symmetric Objects, *ApJ*, 622, 136, doi: [10.1086/427934](https://doi.org/10.1086/427934)
- Guo, F., & Mathews, W. G. 2014, Hot versus Cold: the Dichotomy in Spherical Accretion of Cooling Flows onto Supermassive Black Holes in Elliptical Galaxies, Galaxy Groups, and Clusters, *ApJ*, 780, 126, doi: [10.1088/0004-637X/780/2/126](https://doi.org/10.1088/0004-637X/780/2/126)
- Hardcastle, M. J., & Croston, J. H. 2020, Radio galaxies and feedback from AGN jets, *NewAR*, 88, 101539, doi: [10.1016/j.newar.2020.101539](https://doi.org/10.1016/j.newar.2020.101539)
- Hirose, S., Blaes, O., & Krolik, J. H. 2009, Turbulent Stresses in Local Simulations of Radiation-dominated Accretion Disks, and the Possibility of the Lightman-Eardley Instability, *ApJ*, 704, 781, doi: [10.1088/0004-637X/704/1/781](https://doi.org/10.1088/0004-637X/704/1/781)
- Ito, H., Kino, M., Kawakatu, N., Isobe, N., & Yamada, S. 2008, The Estimate of Kinetic Power of Jets in FR II Radio Galaxies: Existence of Invisible Components?, *ApJ*, 685, 828, doi: [10.1086/591036](https://doi.org/10.1086/591036)
- Ito, H., Kino, M., Kawakatu, N., & Orienti, M. 2015, The Fate of Dead Radio-loud Active Galactic Nuclei: A New Prediction of Long-lived Shell Emission, *ApJ*, 806, 241, doi: [10.1088/0004-637X/806/2/241](https://doi.org/10.1088/0004-637X/806/2/241)
- Kaiser, C. R., & Alexander, P. 1997, A self-similar model for extragalactic radio sources, *MNRAS*, 286, 215, doi: [10.1093/mnras/286.1.215](https://doi.org/10.1093/mnras/286.1.215)
- Kaiser, C. R., Schoenmakers, A. P., & Röttgering, H. J. A. 2000, Radio galaxies with a ‘double-double’ morphology - II. The evolution of double-double radio galaxies and implications for the alignment effect in FR II sources, *MNRAS*, 315, 381, doi: [10.1046/j.1365-8711.2000.03431.x](https://doi.org/10.1046/j.1365-8711.2000.03431.x)
- Kam, M., Hodgson, J. A., Park, J., et al. 2024, Evolution of the Termination Region of the Parsec-scale Jet of 3C 84 Over the Past 20 yr, *ApJ*, 970, 176, doi: [10.3847/1538-4357/ad51dc](https://doi.org/10.3847/1538-4357/ad51dc)
- Kato, S., Fukue, J., & Mineshige, S. 2008, Black-Hole Accretion Disks — Towards a New Paradigm —
- Kawakatu, N., Nagai, H., & Kino, M. 2008, The Fate of Young Radio Galaxies: Decelerations Inside Host Galaxies?, *ApJ*, 687, 141, doi: [10.1086/591900](https://doi.org/10.1086/591900)
- Kawamuro, T., Ueda, Y., Shidatsu, M., et al. 2016, Hard X-ray luminosity function of tidal disruption events: First results from the MAXI extragalactic survey, *PASJ*, 68, 58, doi: [10.1093/pasj/psw056](https://doi.org/10.1093/pasj/psw056)
- Kiehlmann, S., Readhead, A. C. S., O’Neill, S., et al. 2024a, Compact Symmetric Objects. II. Confirmation of a Distinct Population of High-luminosity Jetted Active Galaxies, *ApJ*, 961, 241, doi: [10.3847/1538-4357/ad0cc2](https://doi.org/10.3847/1538-4357/ad0cc2)
- Kiehlmann, S., Lister, M. L., Readhead, A. C. S., et al. 2024b, Compact Symmetric Objects. I. Toward a Comprehensive Bona Fide Catalog, *ApJ*, 961, 240, doi: [10.3847/1538-4357/ad0c56](https://doi.org/10.3847/1538-4357/ad0c56)
- Kino, M., Ito, H., Wajima, K., et al. 2017, Fossil Shell in 3C 84 as TeV γ -Ray Emitter and Cosmic-Ray Accelerator, *ApJ*, 843, 82, doi: [10.3847/1538-4357/aa7336](https://doi.org/10.3847/1538-4357/aa7336)
- Kino, M., & Kawakatu, N. 2005, Estimate of the total kinetic power and age of an extragalactic jet by its cocoon dynamics: the case of Cygnus A, *MNRAS*, 364, 659, doi: [10.1111/j.1365-2966.2005.09580.x](https://doi.org/10.1111/j.1365-2966.2005.09580.x)
- Kino, M., Kawakatu, N., & Ito, H. 2007, Extragalactic MeV γ -ray emission from cocoons of young radio galaxies, *MNRAS*, 376, 1630, doi: [10.1111/j.1365-2966.2007.11354.x](https://doi.org/10.1111/j.1365-2966.2007.11354.x)
- Kino, M., Niinuma, K., Kawakatu, N., et al. 2021, Morphological Transition of the Compact Radio Lobe in 3C 84 via the Strong Jet-Cloud Collision, *ApJL*, 920, L24, doi: [10.3847/2041-8213/ac24fa](https://doi.org/10.3847/2041-8213/ac24fa)

- Komatsu, E., Dunkley, J., Nolte, M. R., et al. 2009, Five-Year Wilkinson Microwave Anisotropy Probe Observations: Cosmological Interpretation, *ApJS*, 180, 330, doi: [10.1088/0067-0049/180/2/330](https://doi.org/10.1088/0067-0049/180/2/330)
- Komissarov, S. S., Barkov, M. V., Vlahakis, N., & Königl, A. 2007, Magnetic acceleration of relativistic active galactic nucleus jets, *MNRAS*, 380, 51, doi: [10.1111/j.1365-2966.2007.12050.x](https://doi.org/10.1111/j.1365-2966.2007.12050.x)
- Kunert-Bajraszewska, M., Gawroński, M. P., Labiano, A., & Siemiginowska, A. 2010, A survey of low-luminosity compact sources and its implication for the evolution of radio-loud active galactic nuclei - I. Radio data, *MNRAS*, 408, 2261, doi: [10.1111/j.1365-2966.2010.17271.x](https://doi.org/10.1111/j.1365-2966.2010.17271.x)
- Kunert-Bajraszewska, M., Wołowska, A., Mooley, K., Kharb, P., & Hallinan, G. 2020, Caltech-NRAO Stripe 82 Survey (CNSS). IV. The Birth of Radio-loud Quasar 013815+00, *ApJ*, 897, 128, doi: [10.3847/1538-4357/ab9598](https://doi.org/10.3847/1538-4357/ab9598)
- Levinson, A., Laor, A., & Vermeulen, R. C. 1995, Constraints on the Parsec-Scale Environment in NGC 1275, *ApJ*, 448, 589, doi: [10.1086/175988](https://doi.org/10.1086/175988)
- Lim, J., Wong, E., Ohyama, Y., Broadhurst, T., & Medezinski, E. 2020, Sustained formation of progenitor globular clusters in a giant elliptical galaxy, *Nature Astronomy*, 4, 153, doi: [10.1038/s41550-019-0909-6](https://doi.org/10.1038/s41550-019-0909-6)
- Lin, D. N. C., & Shields, G. A. 1986, Accretion Disks and Periodic Outbursts of Active Galaxies Nuclei, *ApJ*, 305, 28, doi: [10.1086/164225](https://doi.org/10.1086/164225)
- Lister, M. L., Aller, M. F., Aller, H. D., et al. 2018, MOJAVE. XV. VLBA 15 GHz Total Intensity and Polarization Maps of 437 Parsec-scale AGN Jets from 1996 to 2017, *ApJS*, 234, 12, doi: [10.3847/1538-4365/aa9c44](https://doi.org/10.3847/1538-4365/aa9c44)
- Lister, M. L., Homan, D. C., Kovalev, Y. Y., et al. 2020, TXS 0128+554: A Young Gamma-Ray-emitting Active Galactic Nucleus with Episodic Jet Activity, *ApJ*, 899, 141, doi: [10.3847/1538-4357/aba18d](https://doi.org/10.3847/1538-4357/aba18d)
- Lister, M. L., Cohen, M. H., Homan, D. C., et al. 2009, MOJAVE: Monitoring of Jets in Active Galactic Nuclei with VLBA Experiments. VI. Kinematics Analysis of a Complete Sample of Blazar Jets, *AJ*, 138, 1874, doi: [10.1088/0004-6256/138/6/1874](https://doi.org/10.1088/0004-6256/138/6/1874)
- Machida, M., Hayashi, M. R., & Matsumoto, R. 2000, Global Simulations of Differentially Rotating Magnetized Disks: Formation of Low- β Filaments and Structured Coronalae, *ApJL*, 532, L67, doi: [10.1086/312553](https://doi.org/10.1086/312553)
- Machida, M., & Matsumoto, R. 2003, Global Three-dimensional Magnetohydrodynamic Simulations of Black Hole Accretion Disks: X-Ray Flares in the Plunging Region, *ApJ*, 585, 429, doi: [10.1086/346070](https://doi.org/10.1086/346070)
- MacLeod, M., Guillochon, J., & Ramirez-Ruiz, E. 2012, The Tidal Disruption of Giant Stars and their Contribution to the Flaring Supermassive Black Hole Population, *ApJ*, 757, 134, doi: [10.1088/0004-637X/757/2/134](https://doi.org/10.1088/0004-637X/757/2/134)
- Marecki, A., Spencer, R. E., & Kunert, M. 2003, Location of Weak CSS Sources on the Evolutionary Path of Radio-Loud AGN, *PASA*, 20, 46, doi: [10.1071/AS02051](https://doi.org/10.1071/AS02051)
- Mattila, S., Pérez-Torres, M., Efstathiou, A., et al. 2018, A dust-enshrouded tidal disruption event with a resolved radio jet in a galaxy merger, *Science*, 361, 482, doi: [10.1126/science.aao4669](https://doi.org/10.1126/science.aao4669)
- McClintock, J. E., & Remillard, R. A. 2006, Black hole binaries, 39, 157, doi: [10.48550/arXiv.astro-ph/0306213](https://doi.org/10.48550/arXiv.astro-ph/0306213)
- McCourt, M., Sharma, P., Quataert, E., & Parrish, I. J. 2012, Thermal instability in gravitationally stratified plasmas: implications for multiphase structure in clusters and galaxy haloes, *MNRAS*, 419, 3319, doi: [10.1111/j.1365-2966.2011.19972.x](https://doi.org/10.1111/j.1365-2966.2011.19972.x)
- McNamara, B. R., Rohanizadegan, M., & Nulsen, P. E. J. 2011, Are Radio Active Galactic Nuclei Powered by Accretion or Black Hole Spin?, *ApJ*, 727, 39, doi: [10.1088/0004-637X/727/1/39](https://doi.org/10.1088/0004-637X/727/1/39)
- Meece, G. R., O'Shea, B. W., & Voit, G. M. 2015, Growth and Evolution of Thermal Instabilities in Idealized Galaxy Cluster Cores, *ApJ*, 808, 43, doi: [10.1088/0004-637X/808/1/43](https://doi.org/10.1088/0004-637X/808/1/43)
- Meyer, E. T., Laha, S., Shuvo, O. I., et al. 2024, Emergence of a radio jet in the changing-look AGN 1ES 1927+654, *arXiv e-prints*, arXiv:2406.18061, doi: [10.48550/arXiv.2406.18061](https://doi.org/10.48550/arXiv.2406.18061)
- Mocz, P., Fabian, A. C., & Blundell, K. M. 2011, Inverse-Compton ghosts and double-lobed radio sources in the X-ray sky, *MNRAS*, 413, 1107, doi: [10.1111/j.1365-2966.2011.18198.x](https://doi.org/10.1111/j.1365-2966.2011.18198.x)
- Morganti, R., Murthy, S., Oosterloo, T., et al. 2023, Cold gas in the heart of Perseus A, *A&A*, 678, A42, doi: [10.1051/0004-6361/202347117](https://doi.org/10.1051/0004-6361/202347117)
- Nagai, H., Suzuki, K., Asada, K., et al. 2010, VLBI Monitoring of 3C 84 (NGC 1275) in Early Phase of the 2005 Outburst, *PASJ*, 62, L11, doi: [10.1093/pasj/62.2.L11](https://doi.org/10.1093/pasj/62.2.L11)
- Nagai, H., Orienti, M., Kino, M., et al. 2012, VLBI and single-dish monitoring of 3C 84 for the period 2009-2011, *MNRAS*, 423, L122, doi: [10.1111/j.1745-3933.2012.01269.x](https://doi.org/10.1111/j.1745-3933.2012.01269.x)
- Narayan, R., Chael, A., Chatterjee, K., Ricarte, A., & Curd, B. 2022, Jets in magnetically arrested hot accretion flows: geometry, power, and black hole spin-down, *MNRAS*, 511, 3795, doi: [10.1093/mnras/stac285](https://doi.org/10.1093/mnras/stac285)

- Nath, B. B. 2010, Extended X-ray emission from radio galaxy cocoons, *MNRAS*, 407, 1998, doi: [10.1111/j.1365-2966.2010.17058.x](https://doi.org/10.1111/j.1365-2966.2010.17058.x)
- Nesterov, N. S., Lyuty, V. M., & Valtaoja, E. 1995, Radio and optical evolution of the Seyfert galaxy NGC 1275., *A&A*, 296, 628
- Noda, H., & Done, C. 2018, Explaining changing-look AGN with state transition triggered by rapid mass accretion rate drop, *MNRAS*, 480, 3898, doi: [10.1093/mnras/sty2032](https://doi.org/10.1093/mnras/sty2032)
- Nyland, K., Dong, D. Z., Patil, P., et al. 2020, Quasars That Have Transitioned from Radio-quiet to Radio-loud on Decadal Timescales Revealed by VLASS and FIRST, *ApJ*, 905, 74, doi: [10.3847/1538-4357/abc341](https://doi.org/10.3847/1538-4357/abc341)
- O'Dea, C. P. 1998, The Compact Steep-Spectrum and Gigahertz Peaked-Spectrum Radio Sources, *PASP*, 110, 493, doi: [10.1086/316162](https://doi.org/10.1086/316162)
- O'Dea, C. P., Daly, R. A., Kharb, P., Freeman, K. A., & Baum, S. A. 2009, Physical properties of very powerful FR II radio galaxies, *A&A*, 494, 471, doi: [10.1051/0004-6361:200809416](https://doi.org/10.1051/0004-6361:200809416)
- O'Dea, C. P., & Saikia, D. J. 2021, Compact steep-spectrum and peaked-spectrum radio sources, *A&A Rv*, 29, 3, doi: [10.1007/s00159-021-00131-w](https://doi.org/10.1007/s00159-021-00131-w)
- Orienti, M., & Dallacasa, D. 2020, Variability and parsec-scale radio structure of candidate compact symmetric objects, *MNRAS*, 499, 1340, doi: [10.1093/mnras/staa2856](https://doi.org/10.1093/mnras/staa2856)
- Orienti, M., Murgia, M., & Dallacasa, D. 2010, The last breath of the young gigahertz-peaked spectrum radio source PKS1518+047, *MNRAS*, 402, 1892, doi: [10.1111/j.1365-2966.2009.16016.x](https://doi.org/10.1111/j.1365-2966.2009.16016.x)
- Paraschos, G. F., Kim, J. Y., Krichbaum, T. P., & Zensus, J. A. 2021, Pinpointing the jet apex of 3C 84, *A&A*, 650, L18, doi: [10.1051/0004-6361/202140776](https://doi.org/10.1051/0004-6361/202140776)
- Perucho, M., Quilis, V., & Martí, J.-M. 2011, Intracluster Medium Reheating by Relativistic Jets, *ApJ*, 743, 42, doi: [10.1088/0004-637X/743/1/42](https://doi.org/10.1088/0004-637X/743/1/42)
- Punsly, B., Marziani, P., Bennert, V. N., Nagai, H., & Gurwell, M. A. 2018, Revealing the Broad Line Region of NGC 1275: The Relationship to Jet Power, *ApJ*, 869, 143, doi: [10.3847/1538-4357/aaec75](https://doi.org/10.3847/1538-4357/aaec75)
- Rafferty, D. A., McNamara, B. R., Nulsen, P. E. J., & Wise, M. W. 2006, The Feedback-regulated Growth of Black Holes and Bulges through Gas Accretion and Starbursts in Cluster Central Dominant Galaxies, *ApJ*, 652, 216, doi: [10.1086/507672](https://doi.org/10.1086/507672)
- Ramos Almeida, C., & Ricci, C. 2017, Nuclear obscuration in active galactic nuclei, *Nature Astronomy*, 1, 679, doi: [10.1038/s41550-017-0232-z](https://doi.org/10.1038/s41550-017-0232-z)
- Rawlings, S., & Saunders, R. 1991, Evidence for a common central-engine mechanism in all extragalactic radio sources, *Nature*, 349, 138, doi: [10.1038/349138a0](https://doi.org/10.1038/349138a0)
- Readhead, A. C. S., Hough, D. H., Ewing, M. S., Walker, R. C., & Romney, J. D. 1983, Asymmetric structure in the nuclei of NGC 1275 and 3C 345., *ApJ*, 265, 107, doi: [10.1086/160657](https://doi.org/10.1086/160657)
- Readhead, A. C. S., Xu, W., Pearson, T. J., Wilkinson, P. N., & Polatidis, A. G. 1994, in *Compact Extragalactic Radio Sources*, ed. J. A. Zensus & K. I. Kellermann, 17
- Readhead, A. C. S., Ravi, V., Blandford, R. D., et al. 2024, Compact Symmetric Objects. III. Evolution of the High-luminosity Branch and a Possible Connection with Tidal Disruption Events, *ApJ*, 961, 242, doi: [10.3847/1538-4357/ad0c55](https://doi.org/10.3847/1538-4357/ad0c55)
- Rees, M. J. 1984, Black Hole Models for Active Galactic Nuclei, *ARA&A*, 22, 471, doi: [10.1146/annurev.aa.22.090184.002351](https://doi.org/10.1146/annurev.aa.22.090184.002351)
- Rees, M. J. 1988, Tidal disruption of stars by black holes of 10^6 - 10^8 solar masses in nearby galaxies, *Nature*, 333, 523, doi: [10.1038/333523a0](https://doi.org/10.1038/333523a0)
- Reynolds, C. S., & Begelman, M. C. 1997, Intermittant Radio Galaxies and Source Statistics, *ApJL*, 487, L135, doi: [10.1086/310894](https://doi.org/10.1086/310894)
- Reynolds, C. S., Heinz, S., & Begelman, M. C. 2002, The hydrodynamics of dead radio galaxies, *MNRAS*, 332, 271, doi: [10.1046/j.1365-8711.2002.04724.x](https://doi.org/10.1046/j.1365-8711.2002.04724.x)
- Ricci, C., & Trakhtenbrot, B. 2023, Changing-look active galactic nuclei, *Nature Astronomy*, 7, 1282, doi: [10.1038/s41550-023-02108-4](https://doi.org/10.1038/s41550-023-02108-4)
- Ricci, C., Kara, E., Loewenstein, M., et al. 2020, The Destruction and Recreation of the X-Ray Corona in a Changing-look Active Galactic Nucleus, *ApJL*, 898, L1, doi: [10.3847/2041-8213/ab91a1](https://doi.org/10.3847/2041-8213/ab91a1)
- Ruan, J. J., Anderson, S. F., Eracleous, M., et al. 2019, The Analogous Structure of Accretion Flows in Supermassive and Stellar Mass Black Holes: New Insights from Faded Changing-look Quasars, *ApJ*, 883, 76, doi: [10.3847/1538-4357/ab3c1a](https://doi.org/10.3847/1538-4357/ab3c1a)
- Russell, H. R., McNamara, B. R., Edge, A. C., et al. 2013, Radiative efficiency, variability and Bondi accretion on to massive black holes: the transition from radio AGN to quasars in brightest cluster galaxies, *MNRAS*, 432, 530, doi: [10.1093/mnras/stt490](https://doi.org/10.1093/mnras/stt490)
- Savolainen, T., Giovannini, G., Kovalev, Y. Y., et al. 2023, RadioAstron discovery of a mini-cocoon around the restarted parsec-scale jet in 3C 84, *A&A*, 676, A114, doi: [10.1051/0004-6361/202142594](https://doi.org/10.1051/0004-6361/202142594)

- Scharwächter, J., McGregor, P. J., Dopita, M. A., & Beck, T. L. 2013, Kinematics and excitation of the molecular hydrogen accretion disc in NGC 1275, *MNRAS*, 429, 2315, doi: [10.1093/mnras/sts502](https://doi.org/10.1093/mnras/sts502)
- Shakura, N. I., & Sunyaev, R. A. 1973, Black holes in binary systems. Observational appearance., *A&A*, 24, 337
- Sharma, P., McCourt, M., Quataert, E., & Parrish, I. J. 2012, Thermal instability and the feedback regulation of hot haloes in clusters, groups and galaxies, *MNRAS*, 420, 3174, doi: [10.1111/j.1365-2966.2011.20246.x](https://doi.org/10.1111/j.1365-2966.2011.20246.x)
- Stern, D., McKernan, B., Graham, M. J., et al. 2018, A Mid-IR Selected Changing-look Quasar and Physical Scenarios for Abrupt AGN Fading, *ApJ*, 864, 27, doi: [10.3847/1538-4357/aac726](https://doi.org/10.3847/1538-4357/aac726)
- Sullivan, A. G., Blandford, R. D., Begelman, M. C., Birkinshaw, M., & Readhead, A. C. S. 2024, Small-scale radio jets and tidal disruption events: a theory of high-luminosity compact symmetric objects, *MNRAS*, 528, 6302, doi: [10.1093/mnras/stae322](https://doi.org/10.1093/mnras/stae322)
- Suzuki, K., Nagai, H., Kino, M., et al. 2012, Exploring the Central Sub-parsec Region of the γ -Ray Bright Radio Galaxy 3C 84 with VLBA at 43 GHz in the Period of 2002-2008, *ApJ*, 746, 140, doi: [10.1088/0004-637X/746/2/140](https://doi.org/10.1088/0004-637X/746/2/140)
- Taylor, G. B., Gugliucci, N. E., Fabian, A. C., et al. 2006, Magnetic fields in the centre of the Perseus cluster, *MNRAS*, 368, 1500, doi: [10.1111/j.1365-2966.2006.10244.x](https://doi.org/10.1111/j.1365-2966.2006.10244.x)
- Tchekhovskoy, A., Narayan, R., & McKinney, J. C. 2011, Efficient generation of jets from magnetically arrested accretion on a rapidly spinning black hole, *MNRAS*, 418, L79, doi: [10.1111/j.1745-3933.2011.01147.x](https://doi.org/10.1111/j.1745-3933.2011.01147.x)
- Wajima, K., Kino, M., & Kawakatu, N. 2020, Constraints on the Circumnuclear Disk through Free-Free Absorption in the Nucleus of 3C 84 with KaVA and KVN at 43 and 86 GHz, *ApJ*, 895, 35, doi: [10.3847/1538-4357/ab88a0](https://doi.org/10.3847/1538-4357/ab88a0)
- Walker, R. C., Dhawan, V., Romney, J. D., Kellermann, K. I., & Vermeulen, R. C. 2000, VLBA Absorption Imaging of Ionized Gas Associated with the Accretion Disk in NGC 1275, *ApJ*, 530, 233, doi: [10.1086/308372](https://doi.org/10.1086/308372)
- Wolowska, A., Kunert-Bajraszewska, M., Mooley, K. P., et al. 2021, Caltech-NRAO Stripe 82 Survey (CNSS). V. AGNs That Transitioned to Radio-loud State, *ApJ*, 914, 22, doi: [10.3847/1538-4357/abe62d](https://doi.org/10.3847/1538-4357/abe62d)
- Yang, J., Paragi, Z., van der Horst, A. J., et al. 2016, No apparent superluminal motion in the first-known jetted tidal disruption event Swift J1644+5734, *MNRAS*, 462, L66, doi: [10.1093/mnrasl/slw107](https://doi.org/10.1093/mnrasl/slw107)
- Yuan, F., & Narayan, R. 2014, Hot Accretion Flows Around Black Holes, *ARA&A*, 52, 529, doi: [10.1146/annurev-astro-082812-141003](https://doi.org/10.1146/annurev-astro-082812-141003)
- Zamaninasab, M., Clausen-Brown, E., Savolainen, T., & Tchekhovskoy, A. 2014, Dynamically important magnetic fields near accreting supermassive black holes, *Nature*, 510, 126, doi: [10.1038/nature13399](https://doi.org/10.1038/nature13399)
- Zauderer, B. A., Berger, E., Soderberg, A. M., et al. 2011, Birth of a relativistic outflow in the unusual γ -ray transient Swift J164449.3+573451, *Nature*, 476, 425, doi: [10.1038/nature10366](https://doi.org/10.1038/nature10366)